

ARISTOTLE
UNIVERSITY
OF THESSALONIKI

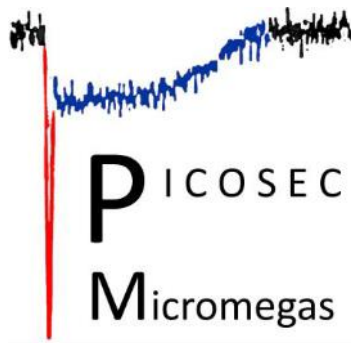
Precise Timing with the PICOSEC Micromegas Detector

Ioannis Manthos

on behalf of the RD51 PICOSEC-Micromegas Collaboration

RD51 PICOSEC-MicroMegas Collaboration

- **CEA Saclay (France):** D. Desforge, I. Giomataris, T. Gustavsson, C. Guyot, F.J. Iguez¹, M. Kebbiri, P. Legou, O. Maillard, T. Papaevangelou, M. Pomorski, P. Schwemlilg, E. Scorsone, L. Sohl
- **CERN (Switzerland):** J. Bortfeldt, F. Brunbauer, C. David, J. Frachi, M. Lupberger, H. Müller, E. Oliveri, F. Resnati, L. Ropelewski, T. Schneider, P. Thuiner, M. van Stenis, R. Veenhof², S.White³
- **USTC (China):** J. Liu, B. Qi, X. Wang, Z. Zhang, Y Zhou
- **AUTH (Greece):** K. Kordas, C. Lampoudis, I. Maniatis, I. Manthos, V. Niaouris, K. Paraschou, D. Sampsonidis, S.E. Tzamarias
- **NCSR (Greece):** G. Fanourakis
- **NTUA (Greece):** Y. Tsiopolitis
- **LIP (Portugal):** M. Gallinaro
- **HIP (Finland):** F. García
- **IGFAE (Spain):** D. González-Díaz



1) Now at Synchrotron Soleil, 91192 Gif-sur-Yvette, France

2) Also MEPhI & Uludag University.

3) Also University of Virginia.

Outline

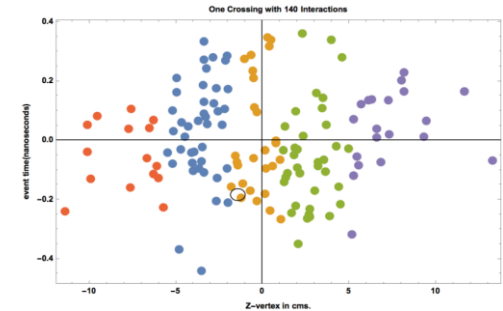
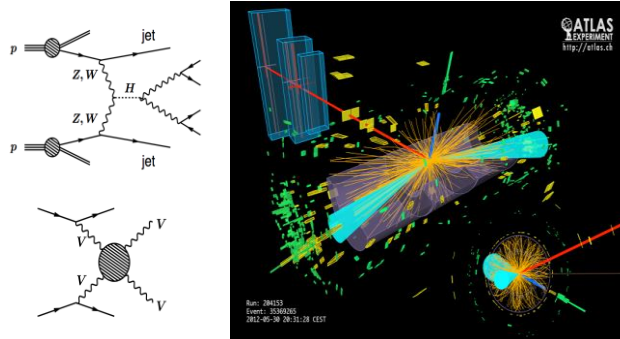
- **PICOSEC MicroMegs: a detector with precise timing**
 - Single-channel prototype in Laser and Particle beams
- **A well-understood detector**
 - Reproduce observed behavior with detailed simulations and a phenomenological model
- **Towards efficient photocathodes**
 - Estimation of the number of photoelectrons per MIP
- **Towards a robust, large-scale detector**
 - Resistive Micromegas, photocathodes, response of multi-channel PICOSEC prototype

Timing with a few 10's of picosecond

- Needs for Precise timing bring us to the **picosec domain**
- E.g., in the **High Luminosity LHC**, 140-200 “pile-up” proton-proton interactions (“vertices”) with happen in the same LHC clock, in close space (Gaussian +/- 45mm).
- Using precise timing can separate particles coming from the various vertices.
- (3D) tracking of charged particles is not enough to associate them to the correct vertex . Including precise time offers an extra dimension of separation to achieve this.
- Needed precision: **order ~30ps**

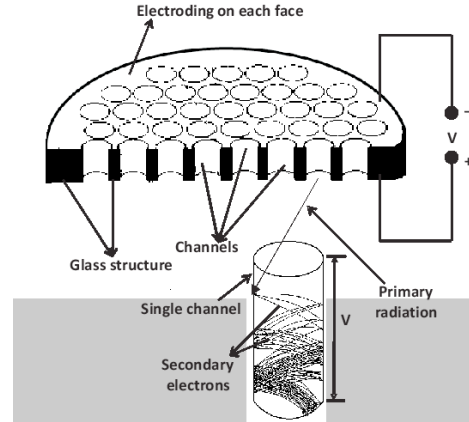


The association of the time measurement to the energy measurement is crucial for physics analysis, and requires time resolution of 20-30ps.

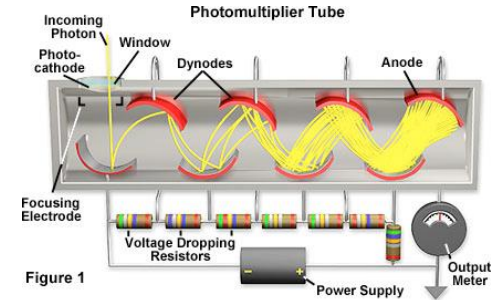


Existing Instrumentation:

e.g. Multi-Channel Plate (MCP) with $\sigma_t \sim 4\text{ps}$ but very expensive for large area coverage



PhotoMultiplier: $\sigma_t > 800\text{ps}$



Since the hermetic approach at the LHC experiments requires large area coverage, it is natural to investigate both MicroPattern Gas and Silicon structures as candidate detector technologies. However, since the necessary time resolution for pileup mitigation is of the order of 20-30 ps, both technologies require significant modification to reach the desired performance.

Large area detectors, resistant to radiation damage, with $\sim 10\text{ps}$ timing capabilities will find applications in many other domains, e.g.

- particle identification in Nuclear and Particle Physics experiments
- photon's energy/speed measurements and correlations for Cosmology
- optical tracking for charge particles
- 4D tracking in the future accelerators (e.g. FCC with a center energy of $\sim 100\text{TeV}$)

MicroMegas: Micro Pattern Gaseous Chambers

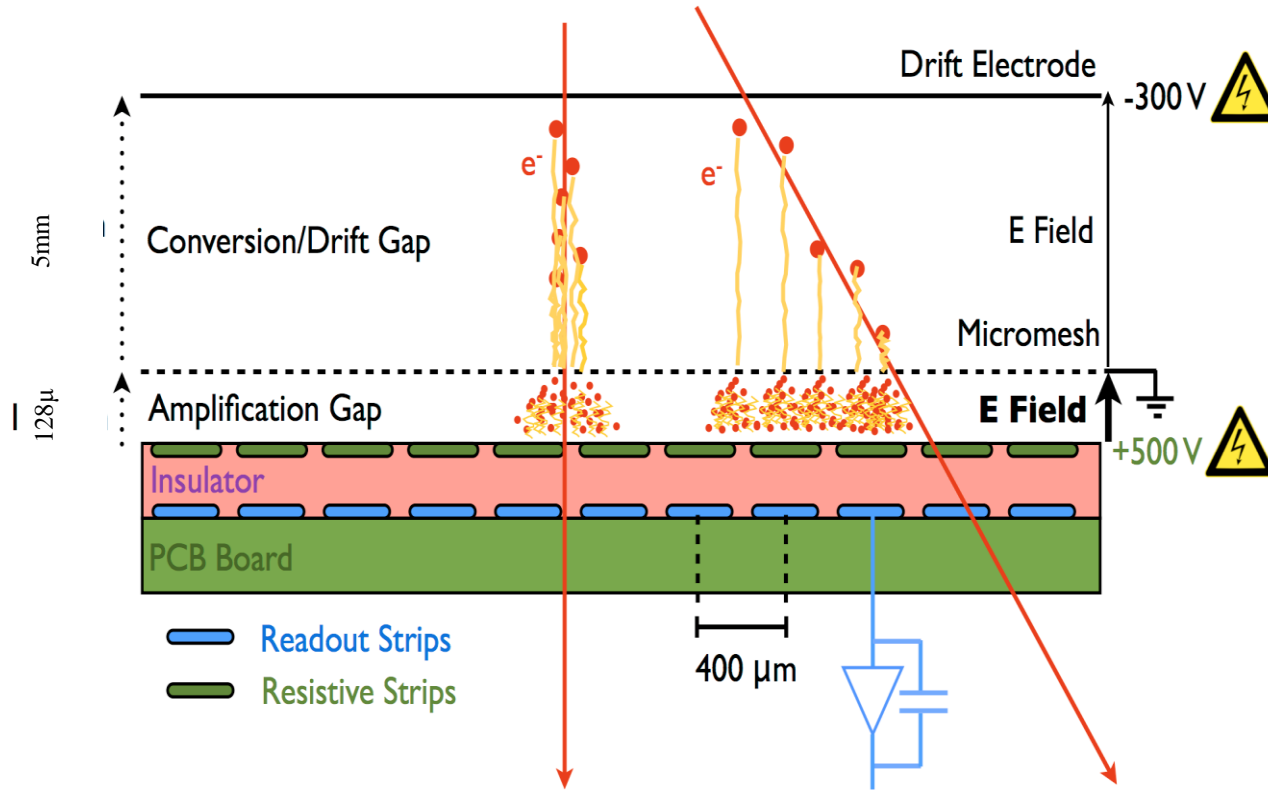
MICROMEAS: a high-granularity position-sensitive gaseous detector for high particle-flux environments

Y. Giomataris^{a,*}, Ph. Rebourgeard^a, J.P. Robert^a, G. Charpak^b

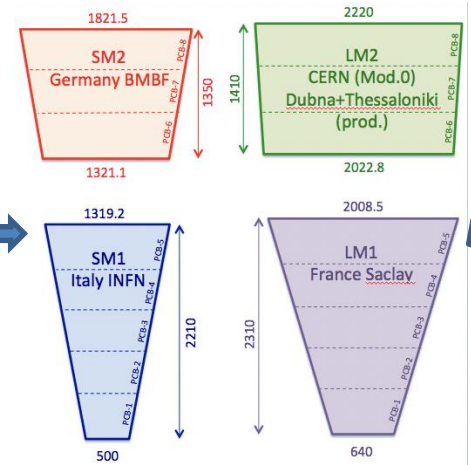
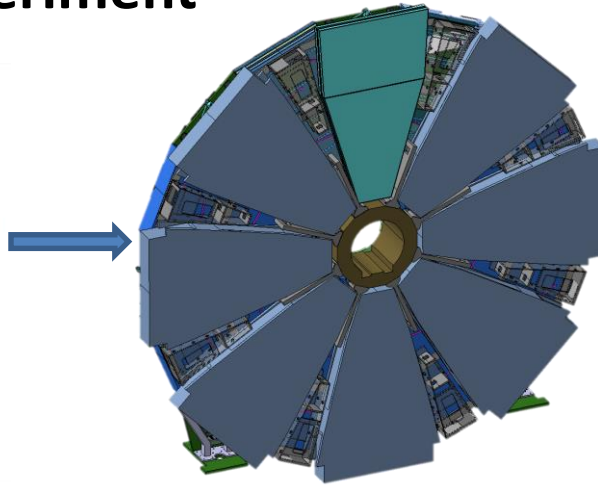
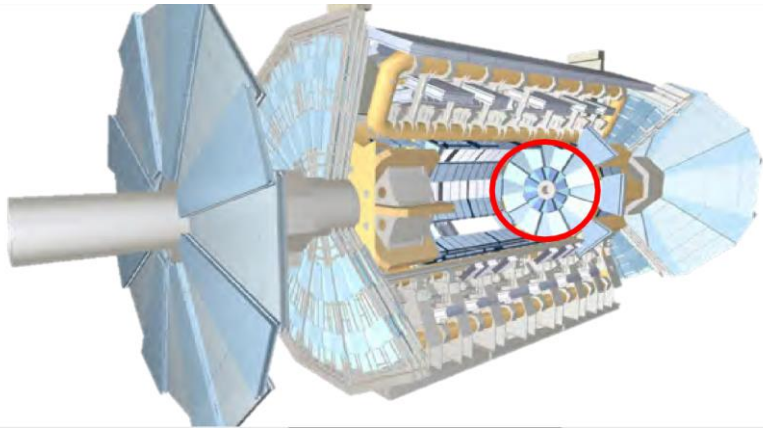
^aCEA/DSM/IMPNA/SED-E-Saclay, 91191 Gif/Yvette, France
^bÉcole Supérieure de Physique et Chimie Industrielle de la ville de Paris, ESPECI, Paris, France
and CERN/AT, Geneva, Switzerland

Received 24 January 1996

[https://doi.org/10.1016/0168-9002\(96\)00175-1](https://doi.org/10.1016/0168-9002(96)00175-1)

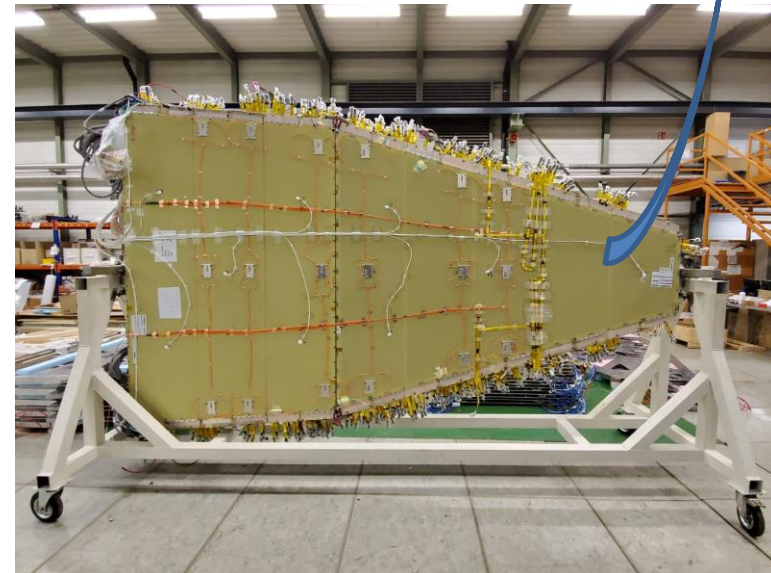


MicroMegas @ ATLAS experiment



Large area coverage: 1200 m²

- Momentum resolution: better than 15% up to $p_t = 1$ TeV
- Single plane resolution: 100 μm , independent from track angle
- Track segment reconstruction: 50 μm
- Track segment efficiency: $\geq 97\%$ @ $p_t > 10$ GeV
- Online angular resolution (trig): ≤ 1 mrad
- Spatial resolution 2nd coordinate: $\sim \text{cm}$, from stereo strips or wires
- Hit rate capability: 15 kHz/cm² (meeting perform. requ.)
- Accumulated charge without ageing: 1 C/cm² (3000 fb⁻¹ w/o degradation)



The Physics of Ionization offers the means for precise spatial measurements (high spatial resolution) but **inhibits precise timing measurements**

ORGANISATION EUROPÉENNE POUR LA RECHERCHE NUCLÉAIRE
CERN EUROPEAN ORGANIZATION FOR NUCLEAR RESEARCH

PRINCIPLES OF OPERATION OF MULTIWIRE
PROPORTIONAL AND DRIFT CHAMBERS

F. Sauli

Lectures given in the
Academic Training Programme of CERN
1975-1976

G E N E V A
1977

10.5170/CERN-1977-009

which is represented in Fig. 8, for $n = 34$, as a function of the coordinate across a 10 mm thick detector. If the time of detection is the time of arrival of the closest electron at one end of the gap, as is often the case, the statistics of ion-pair production set an obvious limit to the time resolution of the detector. A scale of time is also given in the figure, for a collection velocity of 5 cm/ μ sec typical of many gases; the FWHM of the distribution is about 5 nsec. There is no hope of improving this time resolution in a gas counter, unless some averaging over the time of arrival of all electrons is realized.

In order to use gaseous detectors for precise (ps) timing of charged particles we should turn other **Physics** phenomena **against** the stochastic **Nature** of ionization

- Cherenkov radiation \rightarrow provide prompt photons
- Photoelectric effect \rightarrow convert photons to prompt electrons

1. A precise-timing detector

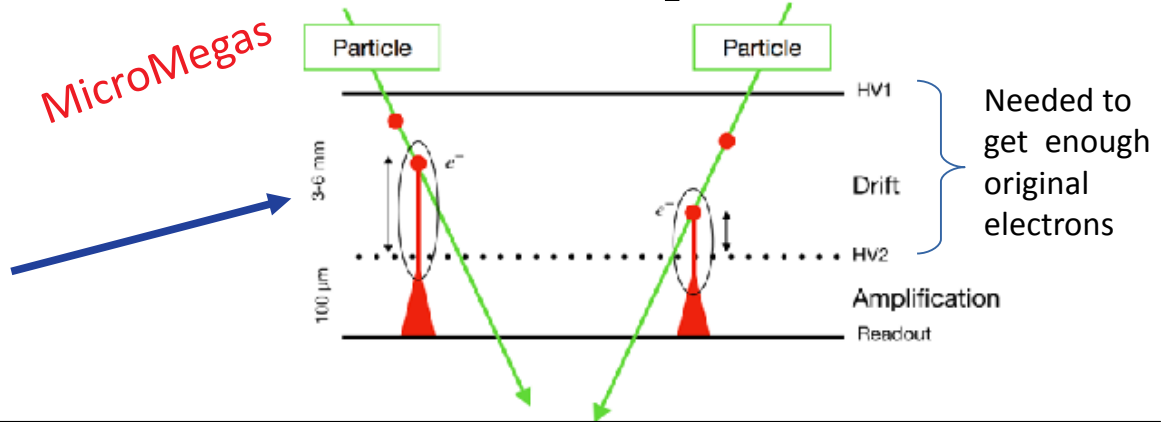
Detector concept and the proof
with results of single-channel prototypes

PICOSEC detector concept

- **Classic Micromegas**

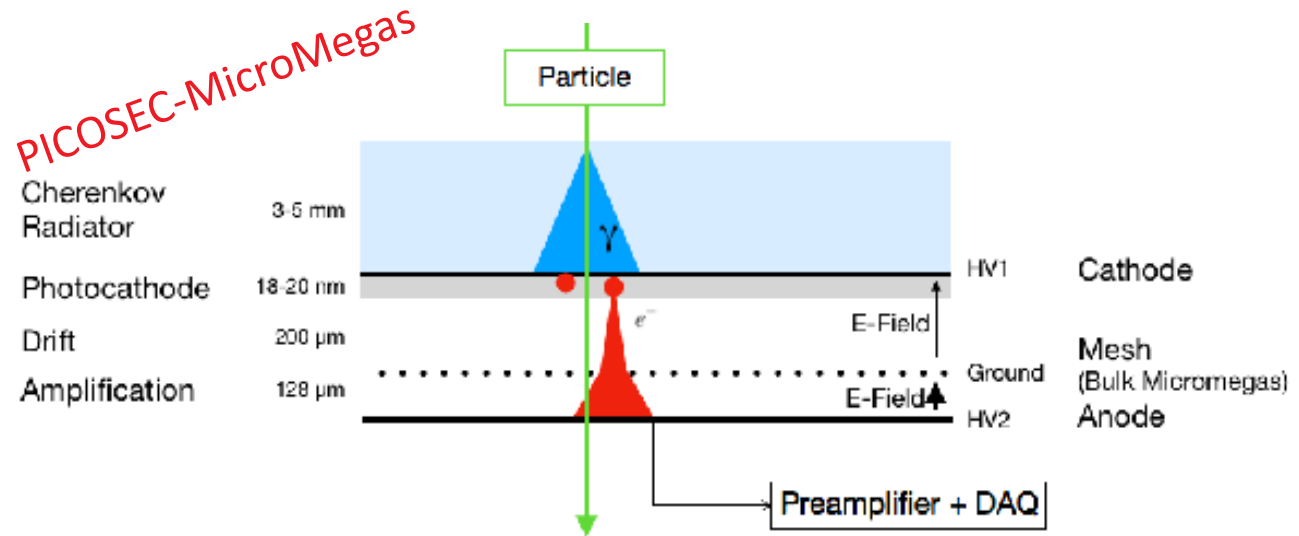
Giomataris Y. et al., NIMA 376(1996) 29

- Multiple electrons produced at different points along particle's path in the $\sim 3\text{-}6\text{mm}$ drift region
 → Time jitter order: **few ns**



- **Micromegas + Cherenkov radiator + photocathode** → synchronous photo-electrons enter Micromegas

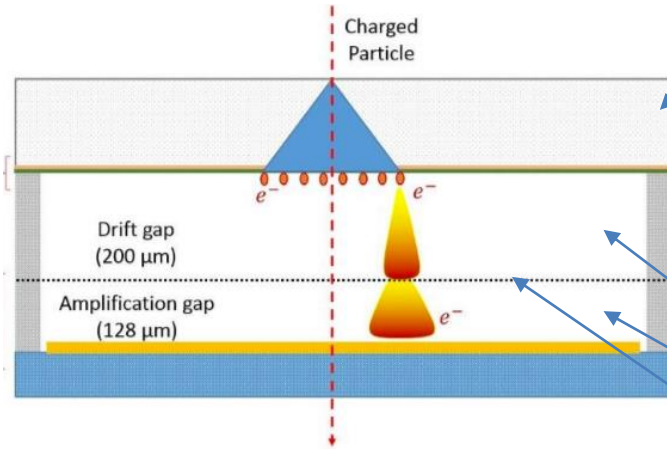
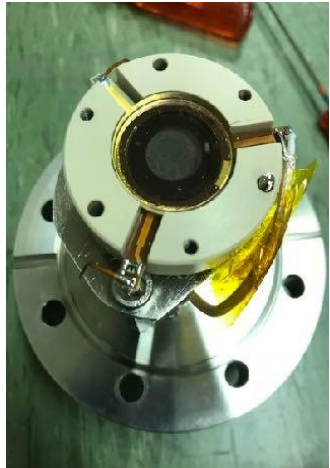
- **Small drift gap & high field** → avalanches start as early as possible with minimal time jitter → Timing resolution a **few tens of ps**



PICOSEC single-channel Prototype

Single pad prototypes - 1 cm diameter active area

st
1 prototype



* Cherenkov Radiator:

MgF₂ 3 mm thick → 3 mm Cherenkov cone

* Photocathode: 18nm CsI (with 5.5 nm Cr - cathode)

* COMPASS gas (80% Ne + 10% CF₄ + 10% C₂H₆)
Pressure: 1 bar.

* Drift gap = 200 μm

* Amplification gap = 128 μm

* Mesh thickness = 36 μm (centered at 128 μm above anode)

Results from Laser and Beam tests presented next are from this detector

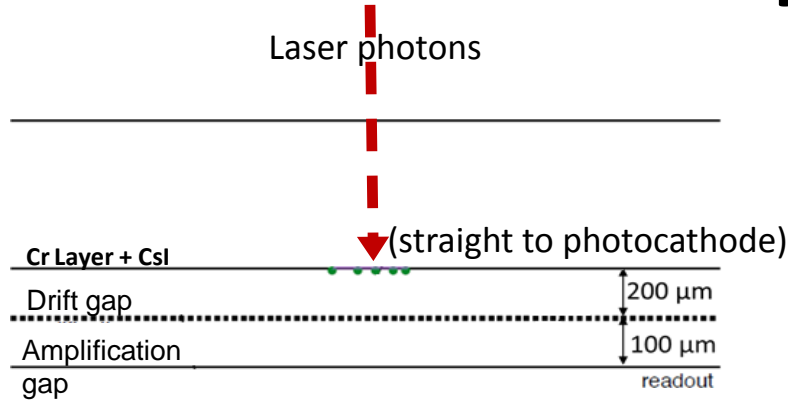
Since 2016, different prototypes studied (bulk, thin mesh etc. MM, multipad MM, different gas, anode schemes, photocathodes)

- Bulk MicroMegas readout (6 pilars)
- 4 kapton rings spacers → 200 μm drift

1a.

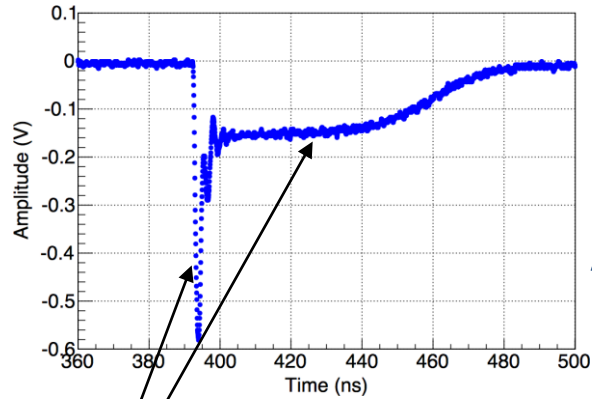
Response to single photoelectrons

Laser beam: response to single electron (1)

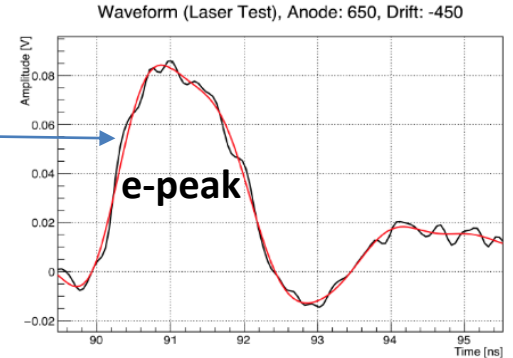
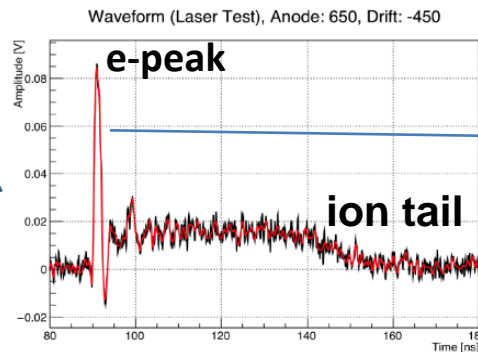


- Pulsed laser at IRAMIS facility (CEA Saclay)
- Wavelength: 267-288 nm
- Repetition rate: up to 500 kHz
- Intensity: attenuated to get single photoelectron directly on photocathode
- Read out with CIVIDEC preamp
- Digitized waveform by 2.5GHz LeCroy oscilloscope @ 20GSamples/s = 1 sample/50ps.
- t_0 reference: fast photodiode (~ 10 ps resolution)

Typical single p.e signal



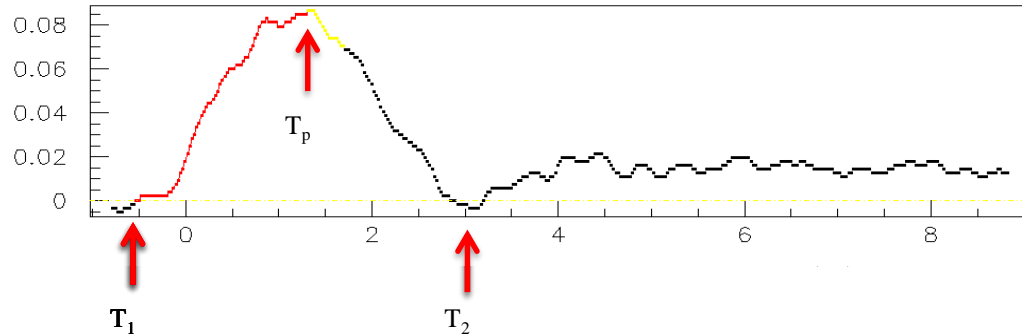
Signal inverted



Two-component signal:

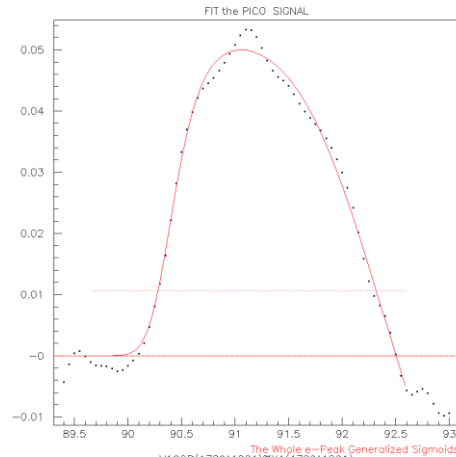
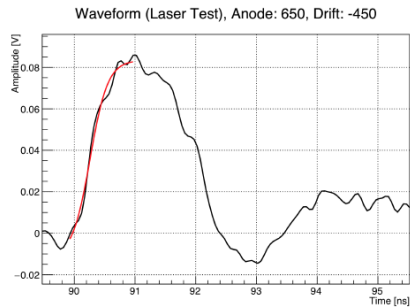
- * Electron peak ("e-peak") \rightarrow fast (~ 0.5 ns)
- * Ion tail \rightarrow slow (~ 100 ns)

Signal processing (1)



- Recognize the “start”, “peak” and “end” of the e-peak
- Evaluate charge by integrating the relevant part
- Fit the e-peak pulse in order to neutralize noise effects using the difference of two logistic functions

$$f(t; p_0, p_1, p_2, p_3, p_4, p_5, p_6) = \frac{p_0}{(1 + e^{-(t-p_1)p_2})^{p_3}} - \frac{p_0}{(1 + e^{-(t-p_4)p_5})^{p_6}}$$



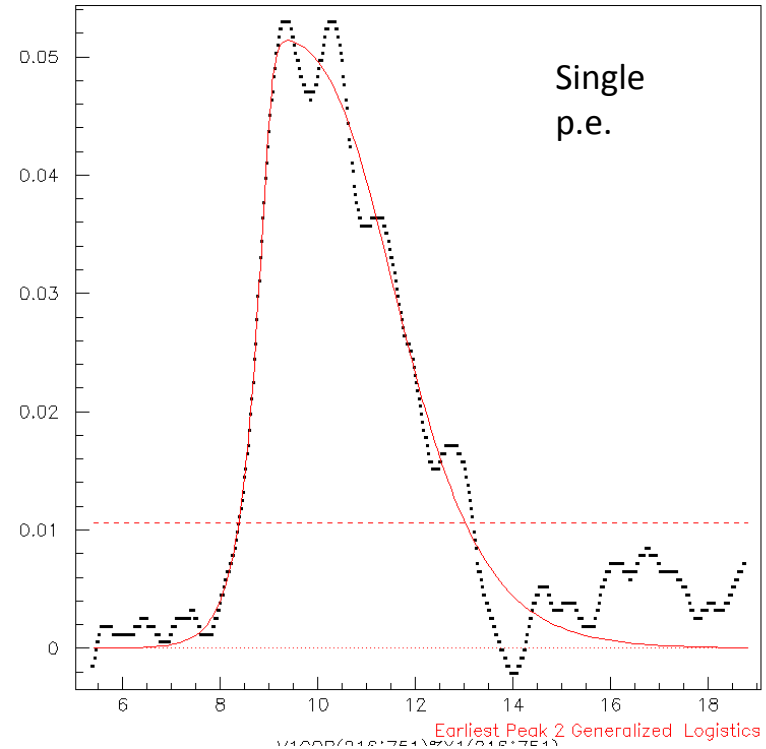
The results of these fit are used to define the “start” and “end” points of the e-peak waveform, to estimate **charge** and it is also used for **timing**

Signal processing (2)

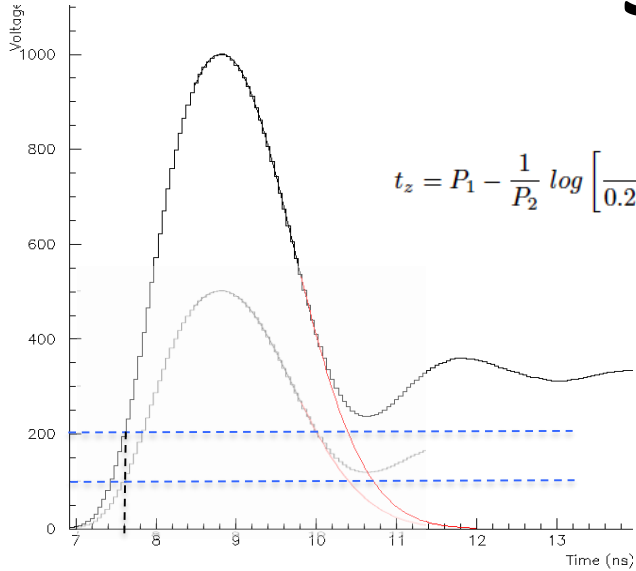
Example: Small pulses

- ✓ Define the start and the end of the e-peak
- ✓ Estimate the charge

Fitting the e-peak waveform helps to estimate the charge in “impossible” cases

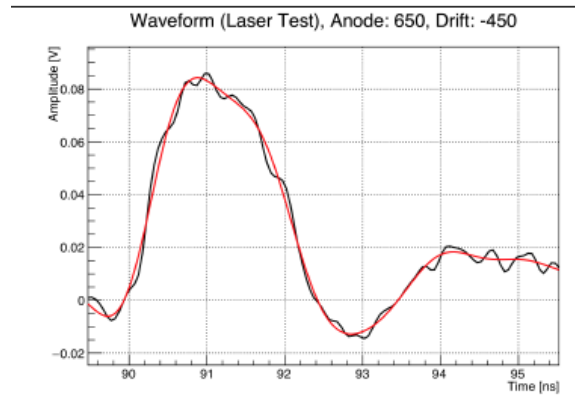
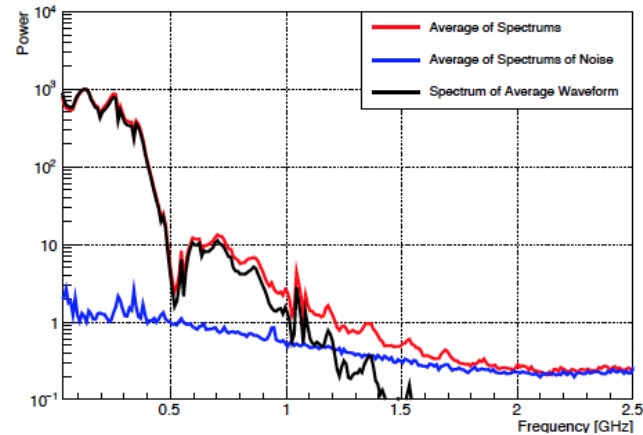


Signal processing (3)



- Define the e-peak arrival time at a Constant Fraction (CFD) of the peak maximum
- CFD Timing minimizes “slewing effects”
- CFD Timing of raw pulses suffers from noise
- Is it possible to filter-out the noise?

An example of filtering out the noise (cut at 1.5 GHz)



Filtering before fitting the leading edge of the pulse **DOES NOT** improve the timing resolution, i.e. a conservative frequency cut does not improve the timing resolution and a strong frequency cut deforms the rising edge of the pulse worsening the time resolution.

Laser beam: response to single electron (2)

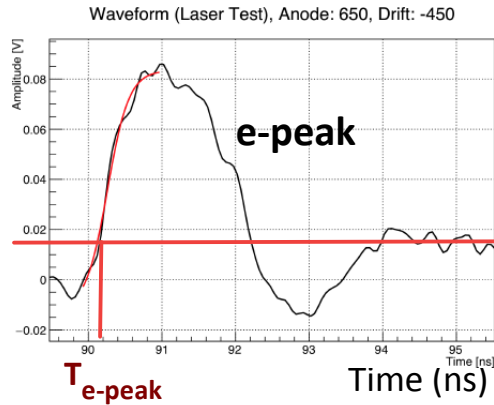
$T_{e\text{-peak}}$ = Signal Arrival Time (SAT)

SAT of a sample of events = $\langle T_{e\text{-peak}} \rangle$

Time Resolution = $\text{RMS}[T_{e\text{-peak}}]$

- t_0 reference: fast photodiode (~ 10 ps resolution)
- Detector response at different field settings

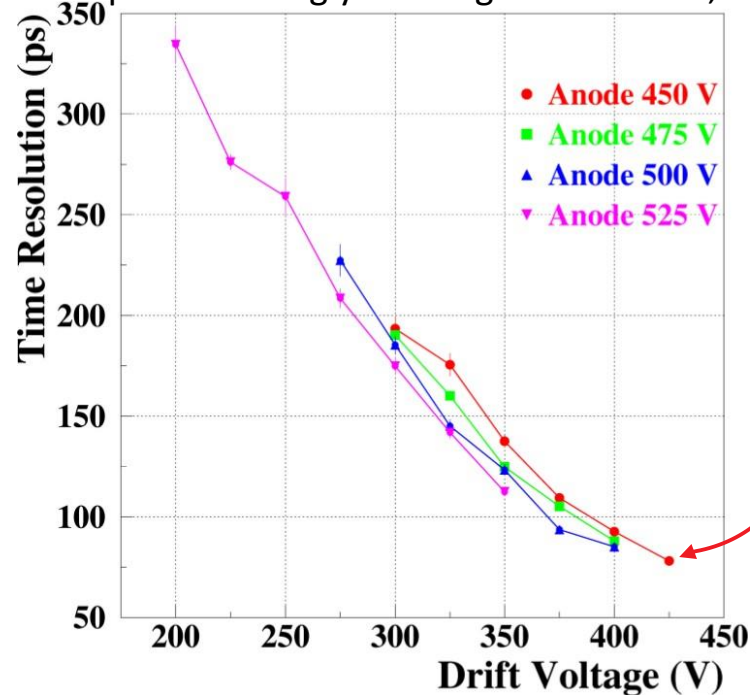
• **Timing resolution 76.0 ± 0.4 ps achieved @ drift/anode: -425V / +450 V**



→ Time the signal arrival with **Constant Fraction Discrimination (CFD)** on the fitted noise-subtracted e-peak

CFD @ 20% of the e-peak amplitude

– improves strongly with higher drift field, less with anode field



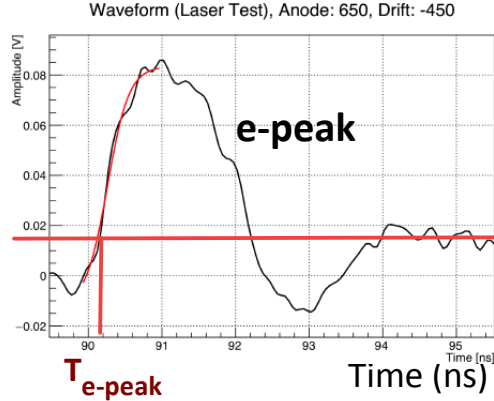
Laser beam: response to single electron (3)

$T_{e\text{-peak}}$ = Signal Arrival Time (SAT)

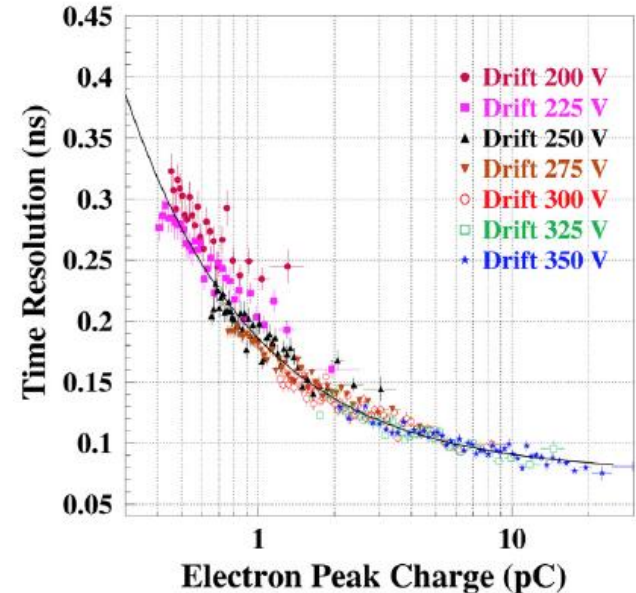
SAT of a sample of events = $\langle T_{e\text{-peak}} \rangle$

Time Resolution = $\text{RMS}[T_{e\text{-peak}}]$

- t_0 reference: fast photodiode (~ 10 ps resolution)
- Detector response at different field settings
- **Timing resolution 76.0 ± 0.4 ps achieved @ drift/anode: -425V / +450 V**
 - improves strongly with higher drift field, less with anode field



Time Resolution depends mostly on e-peak charge

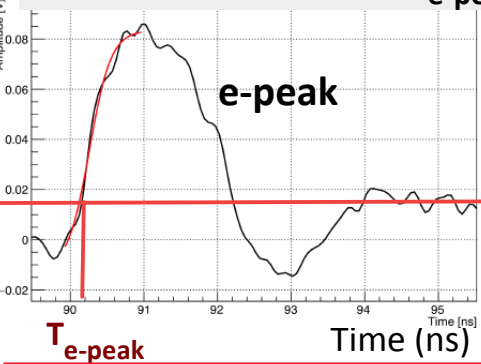


Laser beam: response to single electron (4)

$T_{e\text{-peak}} = \text{Signal Arrival Time (SAT)}$

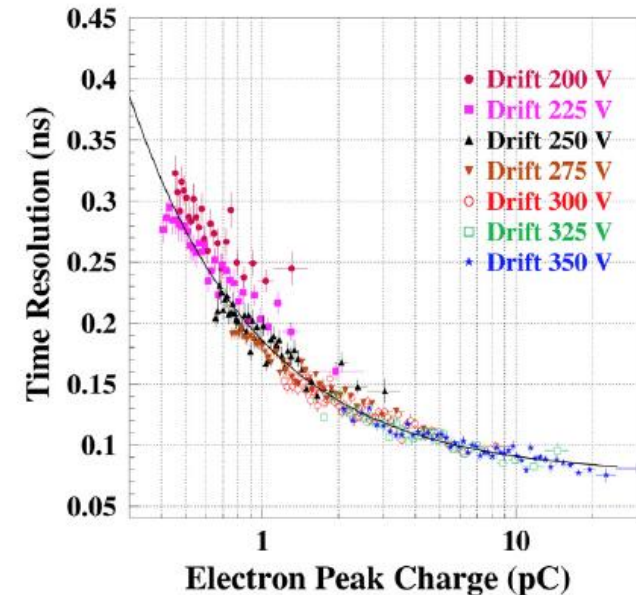
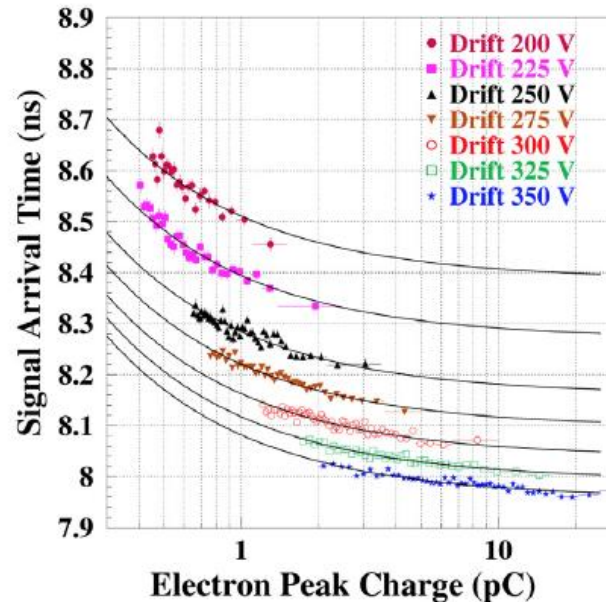
SAT of a sample of events = $\langle T_{e\text{-peak}} \rangle$

Time Resolution = $\text{RMS}[T_{e\text{-peak}}]$



- t_0 reference: fast photodiode (~ 10 ps resolution)
- Detector response at different field settings
- **Timing resolution 76.0 ± 0.4 ps achieved @ drift/anode:**
-425V / +450 V
 - improves strongly with higher drift field, less with anode field

Time Resolution depends mostly on e-peak charge



The Signal Arrival Time (SAT) depends non-trivially on the e-peak charge:

- bigger pulses \rightarrow smaller SAT
- higher drift field \rightarrow smaller SAT

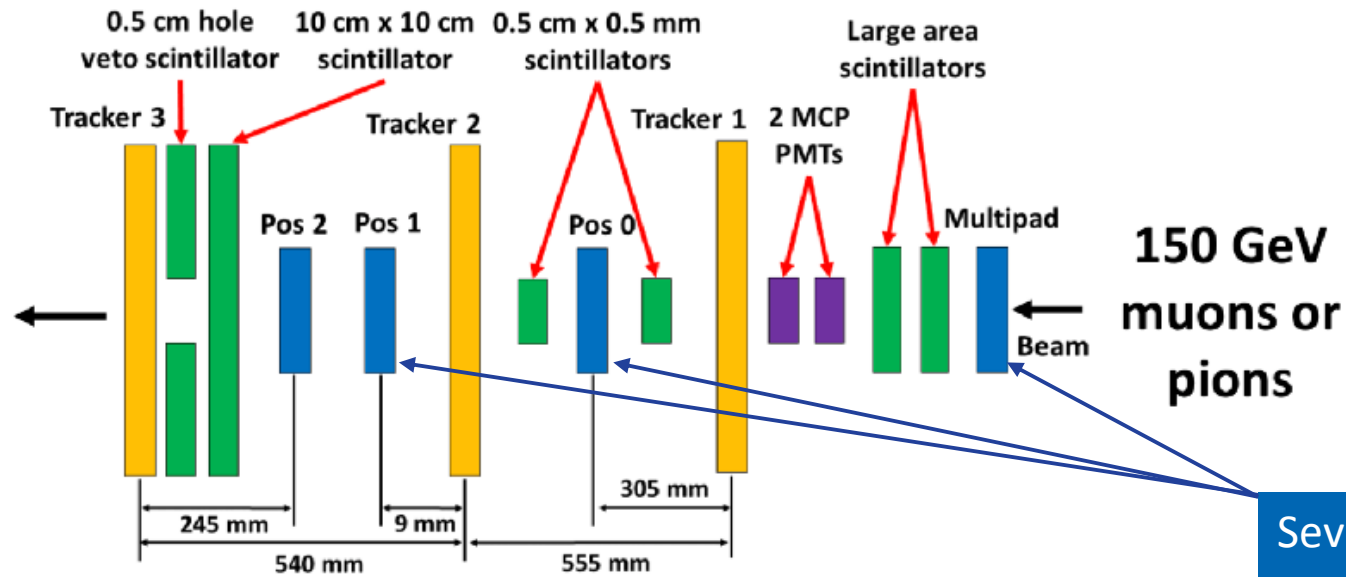
* Shape of pulse is identical in all cases \rightarrow timing with CFD method does not introduce dependence on pulse size

* Responsible for this “slewing” of the SAT:
physics of the detector

1b.

Response to Minimum Ionizing Particles (MIPs)

Testing with Particle Beams @ CERN SPS H4

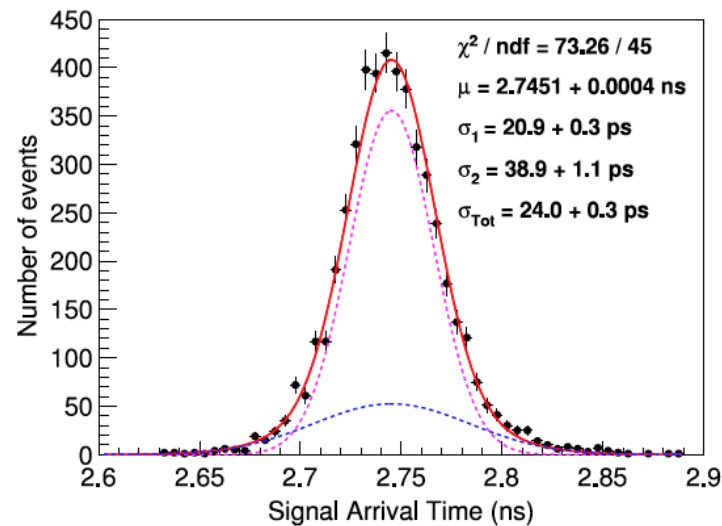
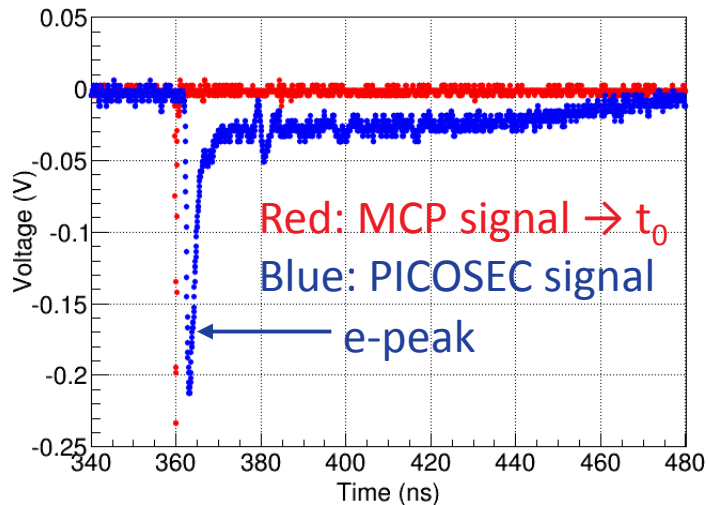


Several PICOSEC prototypes tested in parallel

- **Time reference:** two MCP-PMTs (<5 ps resolution).
- **Scintillators:** used to select tracks & to avoid showers.
- **Tracking system:** 3 triple-GEMs (40 μm precision).
- **Electronics:** CIVIDEC preamp. + 2.5 GHz LeCroy scopes.

Last run Oct. 2018:
The latest for the next
2 years at CERN

Time resolution for MIPs

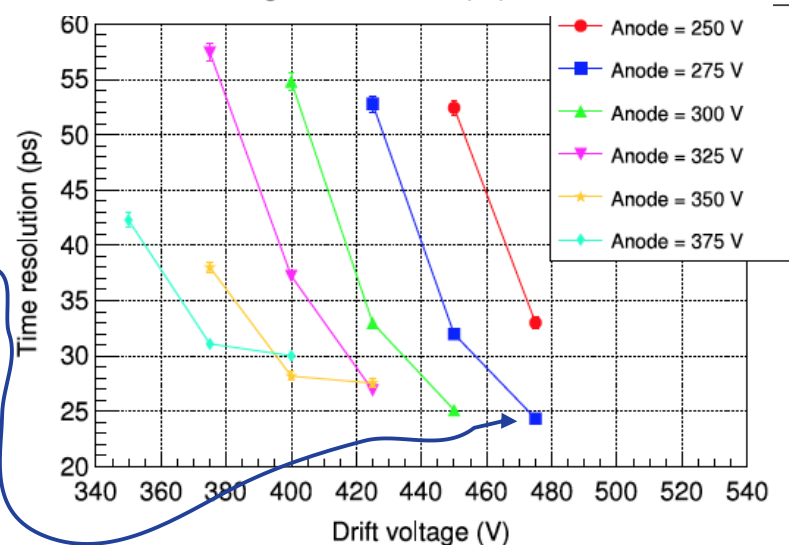


- Same detector as for Laser tests (MgF₂ radiator, CsI photocathode, Bulk MicroMegas, COMPASS gas)

Best time resolution: 24ps 24.0±0.3 ps

- @ Drift/Anode: -475V/+275V

“PICOSEC: Charged particle timing at sub-25 picosecond precision with a Micromegas based detector”, J. Bortfeldt et. al. (RD51-PICOSEC collaboration), Nuclear. Inst. & Methods A 903 (2018) 317-325



2. A well understood detector

detailed simulations and modeling

Detailed simulation with Garfield++ (1)

Use Garfield++ to simulate PICOSEC for single photoelectrons

ANSYS for the electric field

Anode voltage = 450 V

→ E = 35 kV/cm

Cathode voltage = 300-425 V

→ E in [15, 21] kV/cm

Anode voltage does not affect much the timing properties of the signal. So, we split the simulation in three stages:

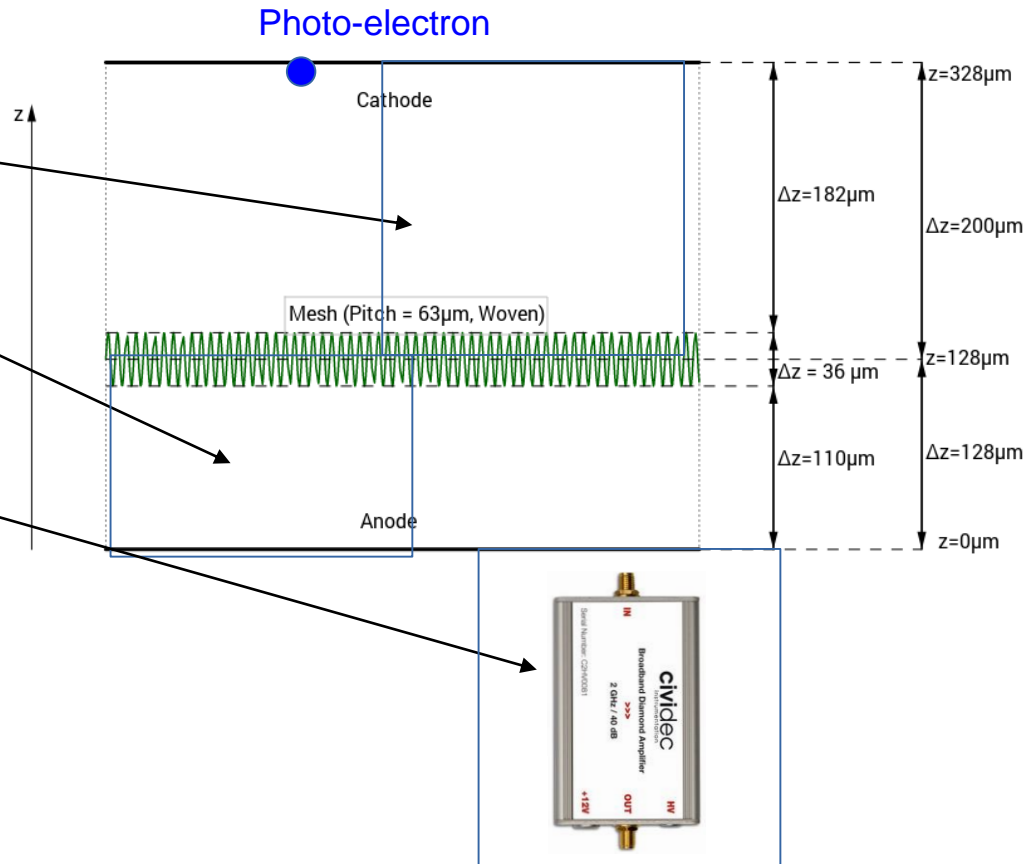
Each photoelectron produces $10^5 - 10^6$ other electrons:

A simulation of the amplification region as well would be very time-consuming (~months, to cover the various voltage etc settings tried).

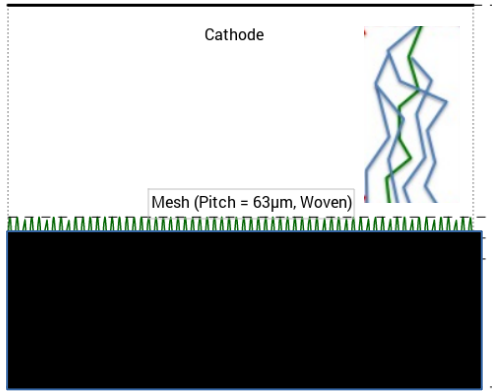
1) Drift region: simulation till the mesh.

2) Simulation in the amplification region

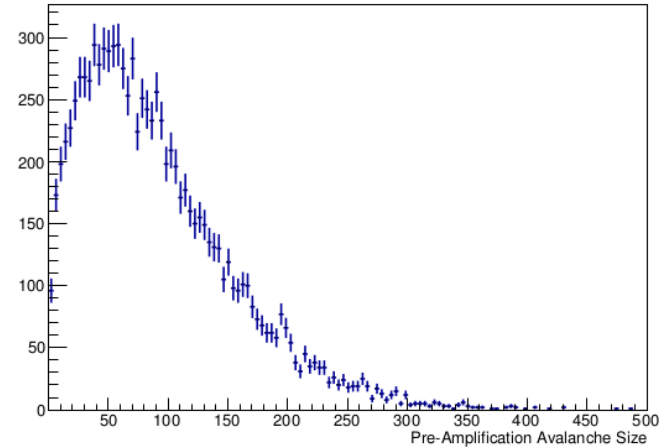
3) Electronics



Detailed simulation with Garfield++ (2)



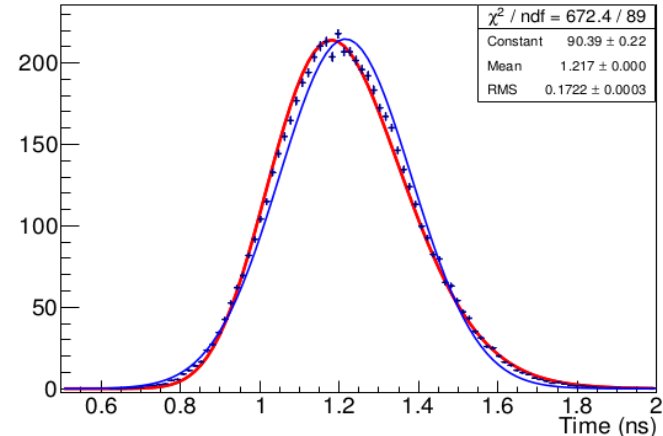
Stage 1 – Drift region



We start with one photoelectron,
and we follow the avalanche it creates
till the mesh.

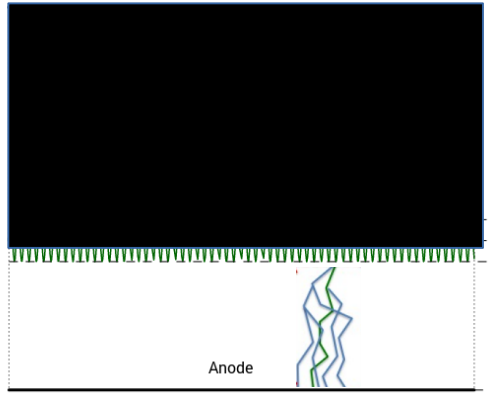
We then count:

- **how many** electrons pass the mesh and **when**

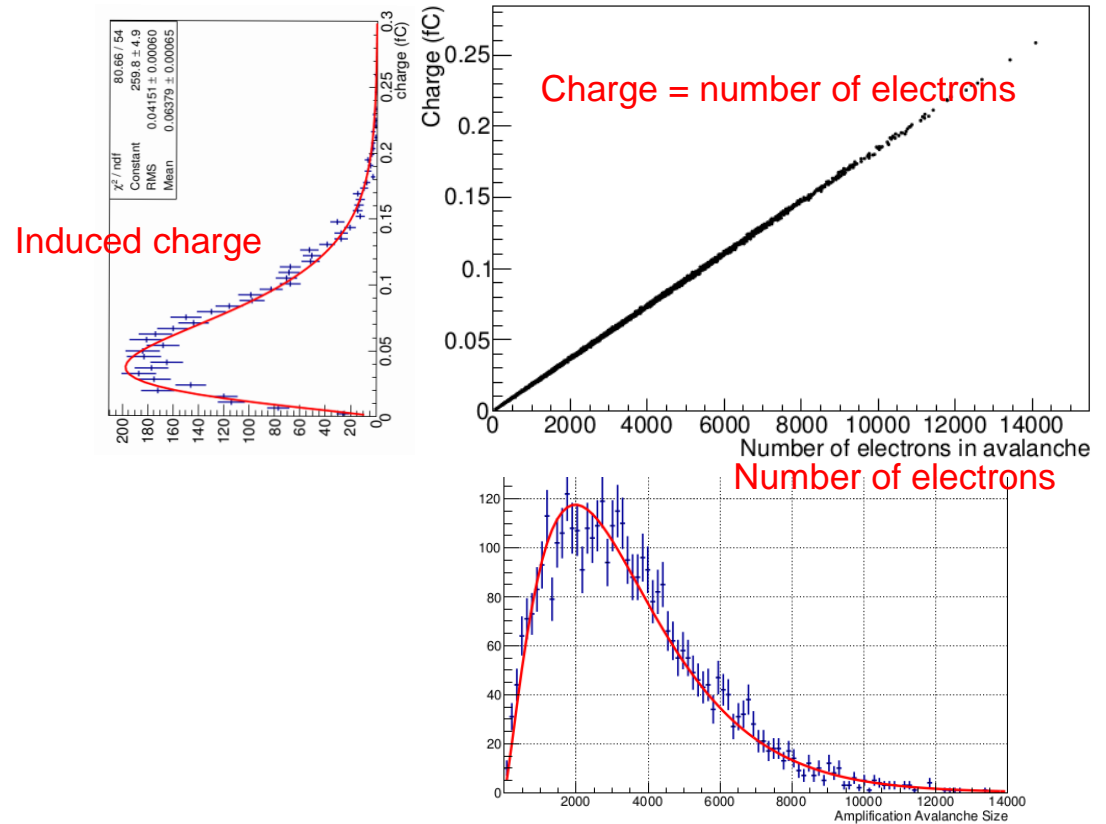


Detailed simulation with Garfield++ (3)

Stage 2 – Amplification Region



We start from an electron which just passed through the mesh, we follow the avalanche it produces in the amplification region, and we count **how many electrons** arrive on the anode and the **induced charge**: **one-to-one correspondence.**



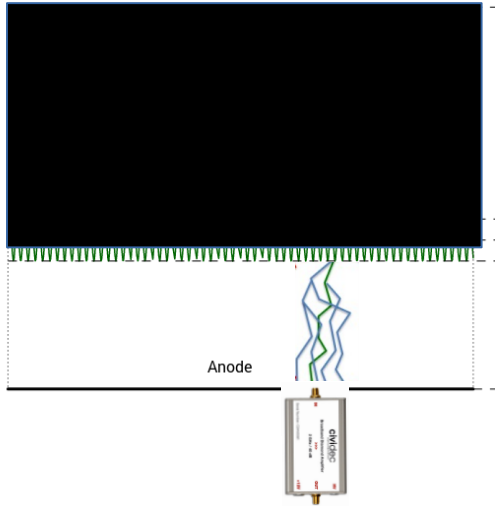
The distribution fit nicely with a Polya (red)

→ for each electron passing the mesh, we can get a representative number of electrons on the anode, by picking randomly from this Polya. 26

Detailed simulation with Garfield++ (4)

Stage 3 – Response of electronics

- Assume that the simulated pulse will be described with the difference of two logistics
- Find the parameters by using experimental data, in a statistically coherent way:
 - a) Describe the pulse shape produced from one electron passing the mesh and entering the amplification region. Take distributions of “mean arrival times” for the electrons reaching the anode (from Garfield++) and convolute them with the shape of the electronic response, and
 - b) Compare the result with the average waveform observed in the experimental data.



$$\frac{\langle S(t) \rangle_{Q_{tot}=Q}}{Q} = \int_0^{\infty} f(t - \tau) \langle \Phi(\tau) \rangle_{Q_{tot}=Q} d\tau$$

Normalized waveform

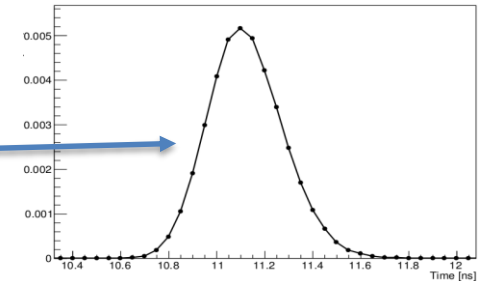
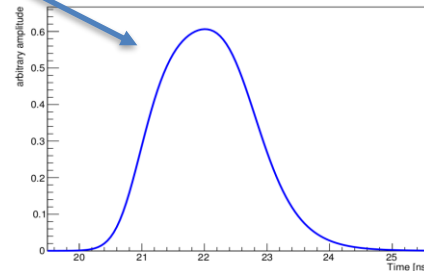
Average waveform
its total charge

= Response function of (convolution)
the electronics *
with all gains=1

Distribution of
Mean Arrival times

(from the simulation)

(from the experimental data)



Detailed simulation with Garfield++ (5)

Pulse generation in Garfield++ –no extra electronic gain

N electrons pass through the mesh at times $\tau_1, \tau_2, \dots, \tau_N$

Each one of these N electrons contributes a pulse $f(t)$ (previous slide),
displaced by the respective time $\tau_1, \tau_2, \dots, \tau_N$,

where the size of the pulse is put as a random variable drawn from the
Polya describing the avalanche population (or the induced charge,
equivalently).

$$S(t) = \sum_{i=1}^N q_i \cdot f(t - \tau_i)$$

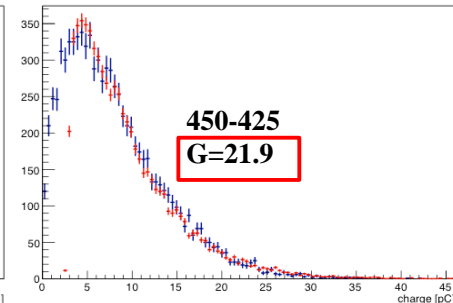
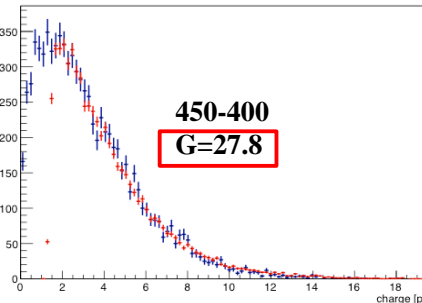
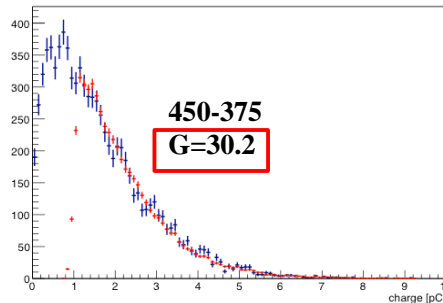
We thus, produce pulses with shapes like those in the experiment, but:

$f(t-\tau_i)$ is the shape of the electronics response: in order the simulated pulses to be exactly like in the data, we need the Gain, G, of the electronics in order to construct $G \cdot S(t)$

Pulse generation in Garfield++ – including electronic gain

G should be a constant. But...

Experiment
Simulation

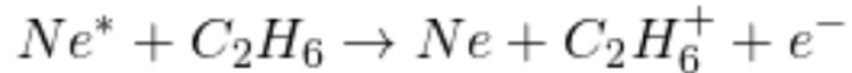


Detailed simulation with Garfield++ (6)

→ There must be another phenomenon not included here...

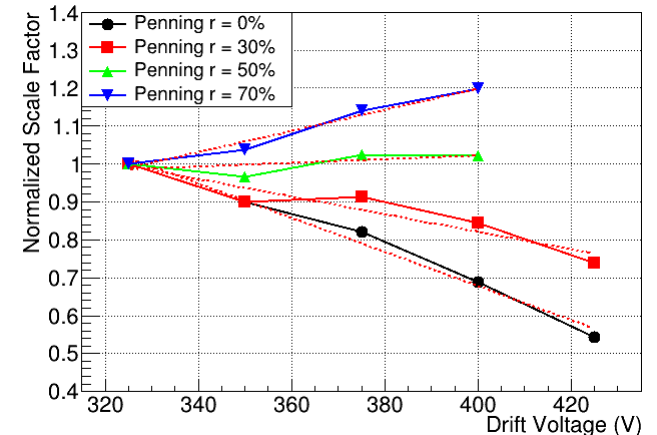
In Garfield++ , all interactions between electrons and molecules are included, but not between molecules themselves.

But Ne has excited states at high enough energies, that, when de-exciting, can cause the ionization of C_2H_6 .

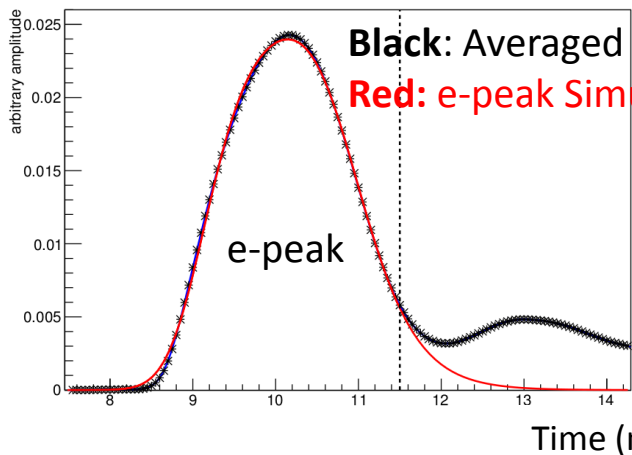


Such indirect ionizations are called the “**Penning effect**”

By putting as a free parameter, the probability, r , to have such an excited Ne to cause an ionization, we found that the value of $r=50\%$ for the “**Penning Transfer Rate**” allows to use a constant electronic gain G , independent of the voltage in the drift region.



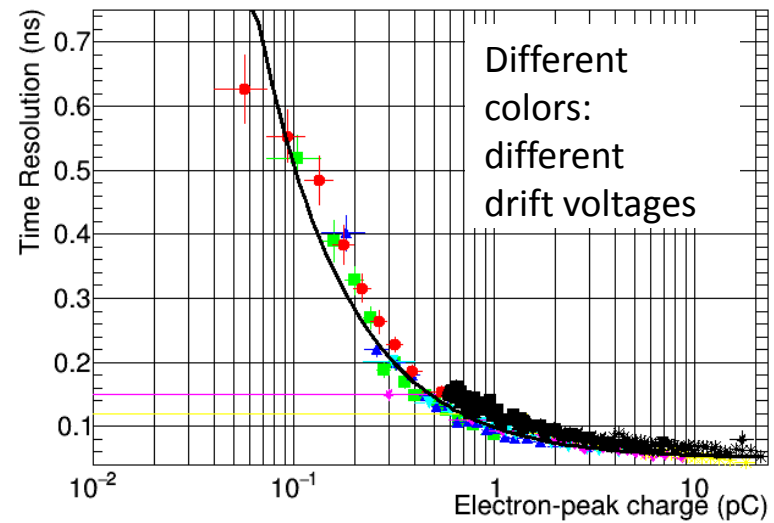
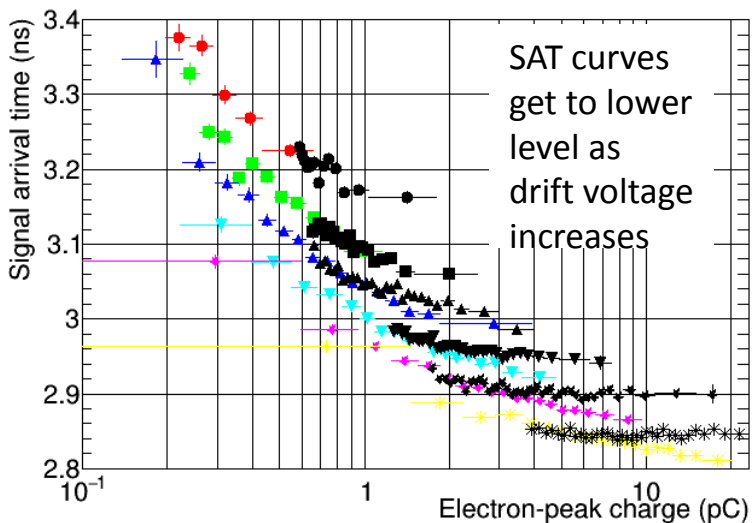
Detailed simulation with “trimmed” Garfield++



All behaviors seen in single p.e. laser data are also seen in these detailed Garfield++ simulations!!!

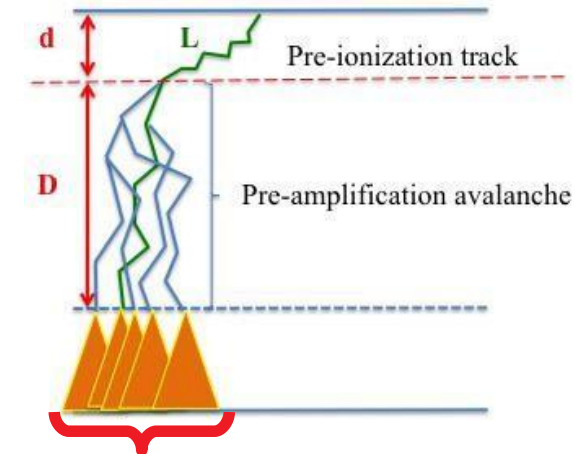
The Signal Arrival Time (SAT) depends non-trivially on the e-peak size:

- * bigger pulses → smaller SAT
- * higher drift field → smaller SAT
- * Time resolution depends mostly on e-peak charge



Color: Simulation – Black: Data

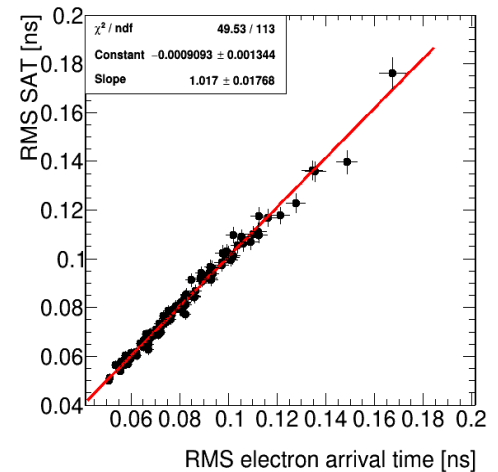
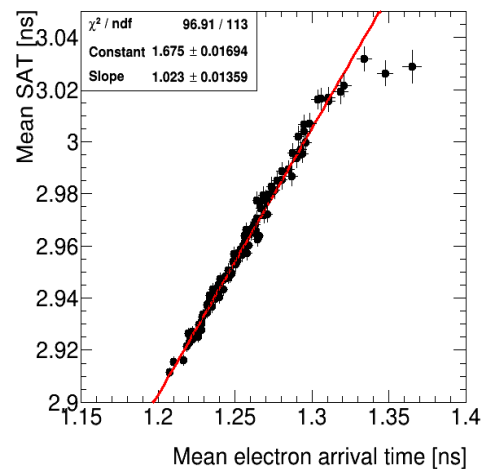
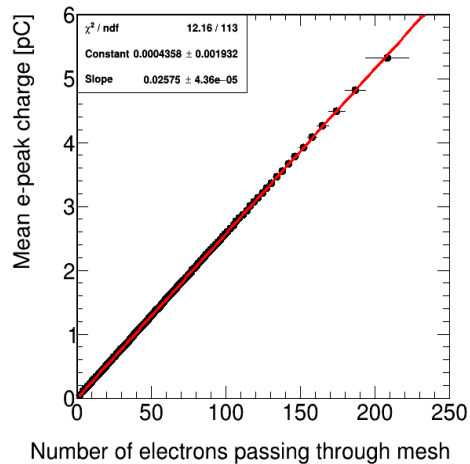
Detailed simulations: under the hood



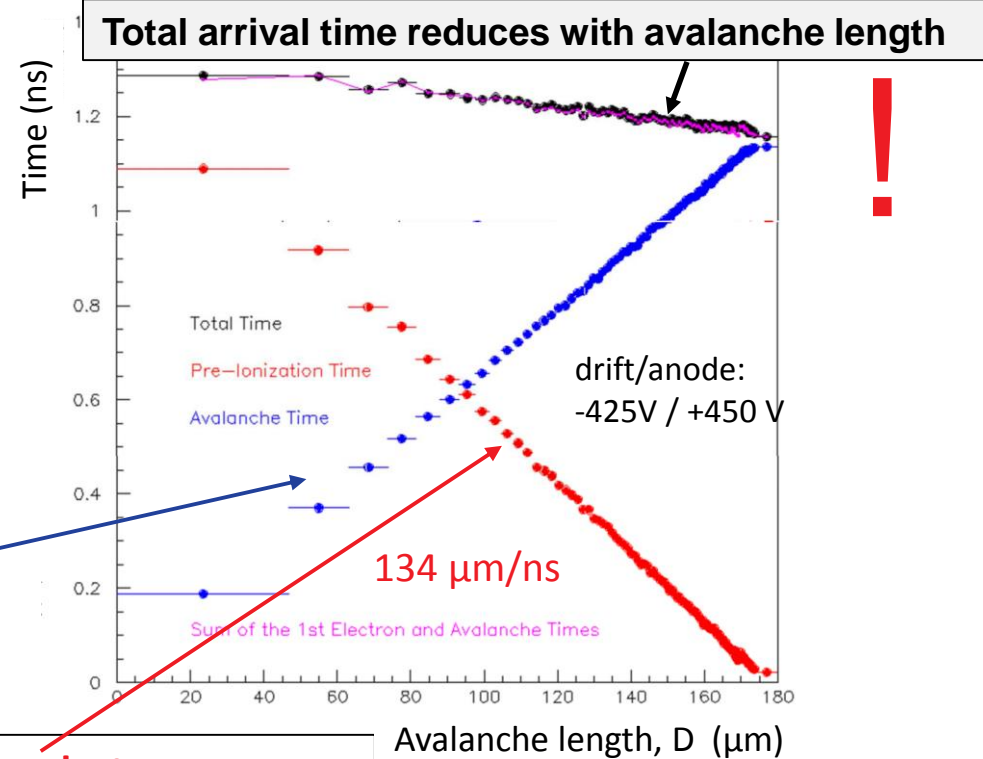
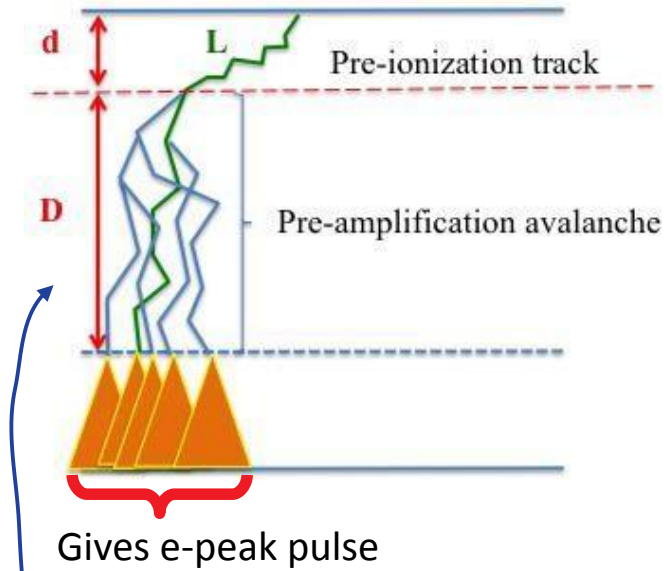
Gives e-peak pulse

Microscopic equivalent to e-peak's SAT = Mean Time (T) of all electron arrival times on the mesh
 * $\langle \text{SAT} \rangle$ linear with $\langle T \rangle$
 * $\text{RMS}(\text{SAT})$ linear with $\text{RMS}(T)$

Correspondence of experimental Observables to Relevant Microscopic Variables
 Sets of avalanches of a certain e-peak charge



Detailed simulations: under the hood



Avalanche runs with higher drift velocity than **pre-ionization electron**

So, SAT "slewing" seen in single p.e data is explained:

SAT reduces with avalanche length

Long avalanches → big e-peak charge } **SAT reduces with e-peak charge**

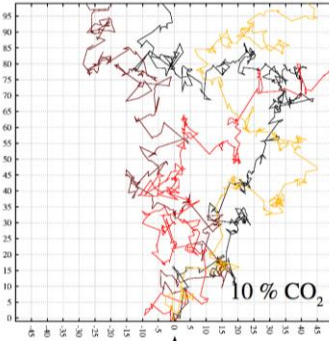
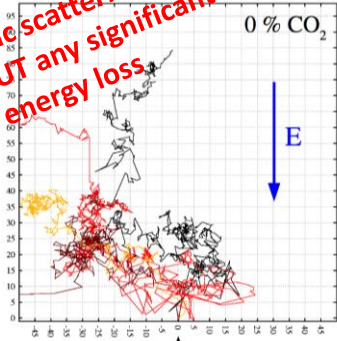
More counter-intuitive observations found related to collective, emerging properties of the avalanche!!

Let us be inspired by the phenomenon of “Quenching”

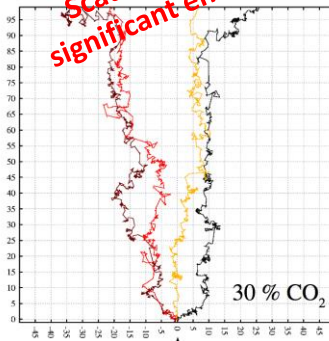
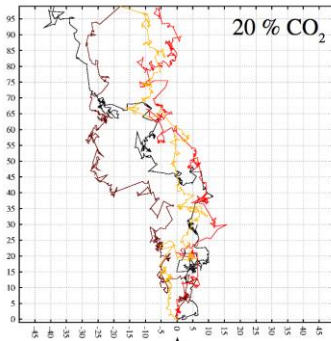
From Rob Veenhof

Electrons in Ar/CO₂ at E=1 kV/cm

Elastic scatterings
WITHOUT any significant
energy loss



Scatterings WITH
significant energy loss



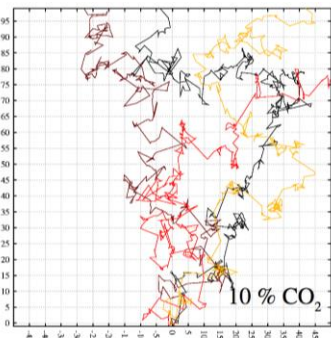
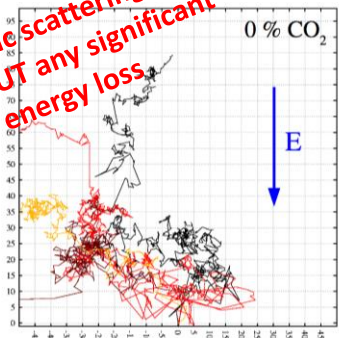
In the case of “quenching”, the energy loss results in higher drift velocity !!!

Let us be inspired by the phenomenon of “Quenching”

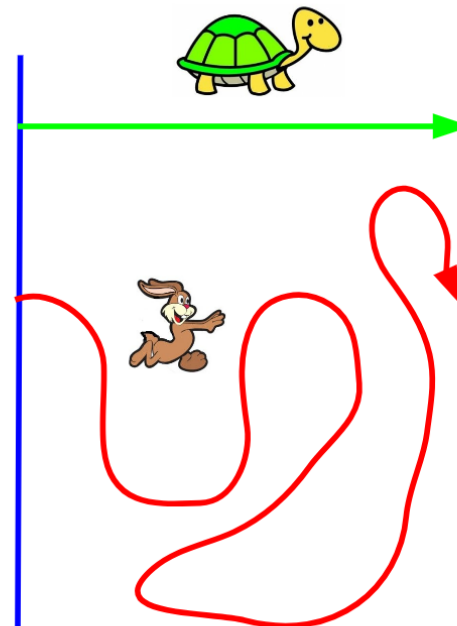
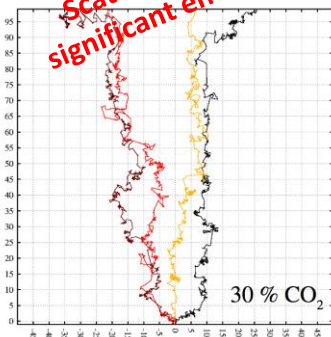
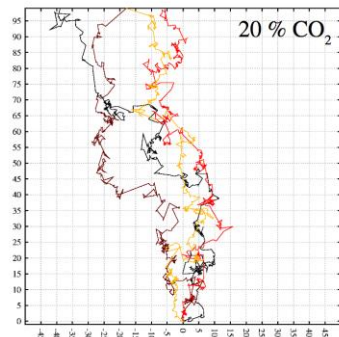
From Rob Veenhof

Electrons in Ar/CO₂ at E=1 kV/cm

Elastic scatterings
WITHOUT any significant
energy loss



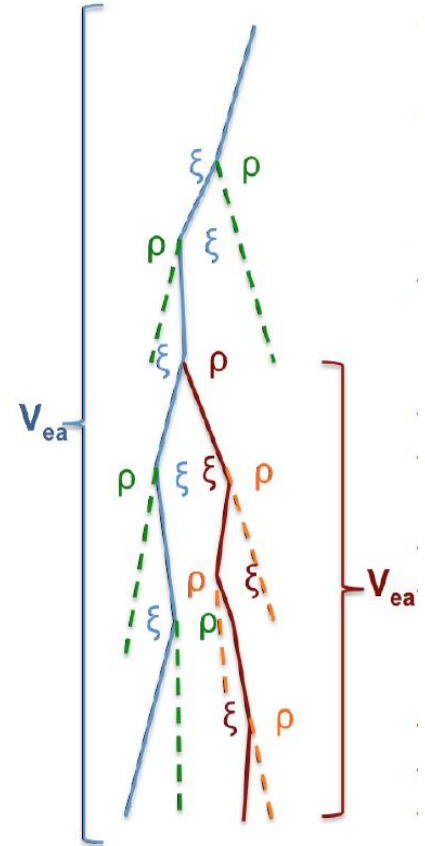
Scatterings WITH
significant energy loss



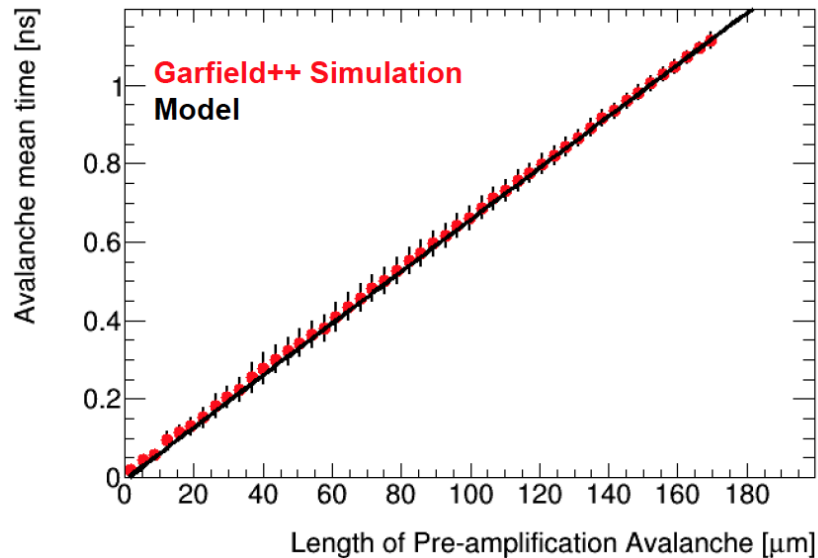
In the case of “quenching”, the energy loss results in higher drift velocity !!!

Phenomenological model: A deeper looking under the hood

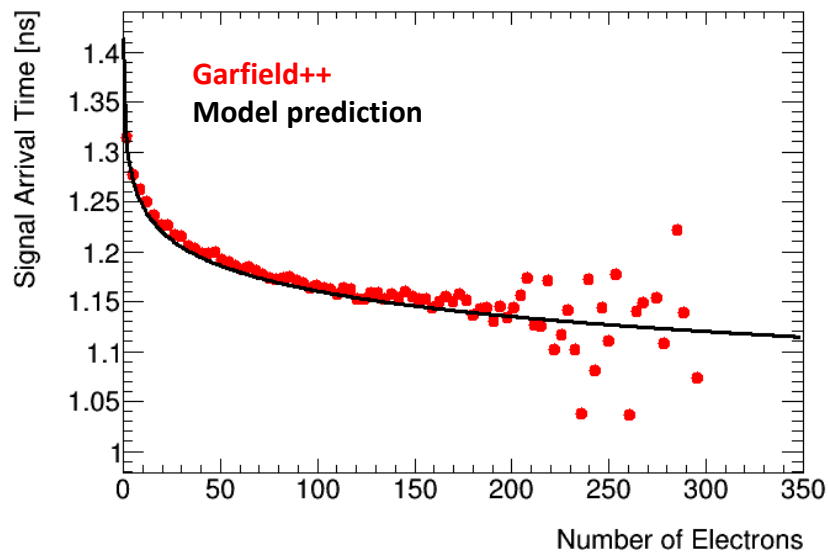
- An ionizing electron in the avalanche, every time it ionizes, will gain a time ξ_i relative to an electron that undergoes elastic scatterings only.
- A new produced electron by ionization starts with low energy, suffers less delay due to elastic backscattering compared to its parent. Relative to his parent it will have a time-gain ρ_i
- Parameters ξ_i and ρ_i should follow a joint probability distribution determined by the physical process of ionization and the respective properties of interacting molecules
 - The collective effect of time-gains ξ_i , is a change in drift velocity from V_p , which is the photoelectron drift velocity before ionization, to an effective drift velocity V_{ea} , which is the drift velocity of an ionizing electron in the avalanche. By taking V_{ea} to be the drift velocity of any electron in the avalanche, the energy-loss effect on the drift of the parent has been taken into account.
 - When a new electron is produced in the avalanche, through ionization, it will gain time ρ_i , at its production, which is assumed to follow a distribution with mean value ρ and variance w^2 . From that moment onwards, this new electron propagates with drift velocity V_{ea} as any other existing electron in the avalanche.



Understood in terms of phenomenological model



We can predict the effective drift velocity of the avalanche

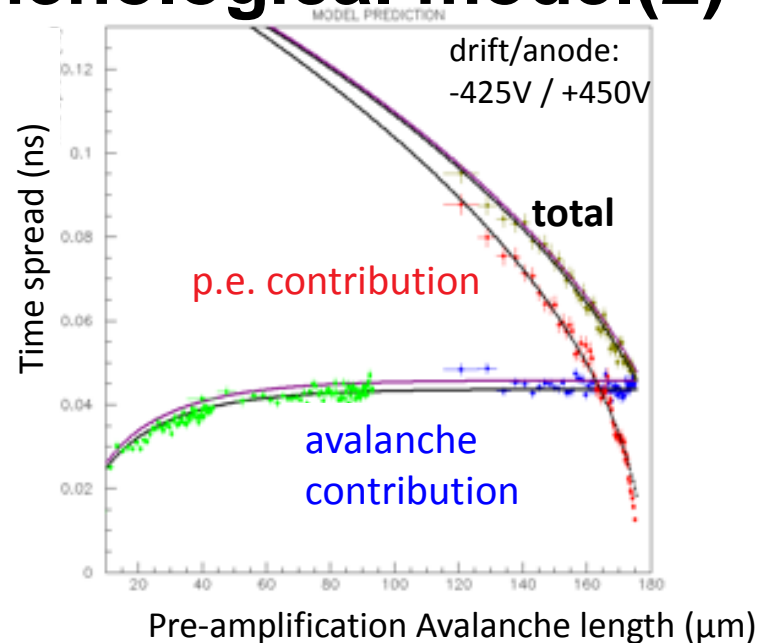
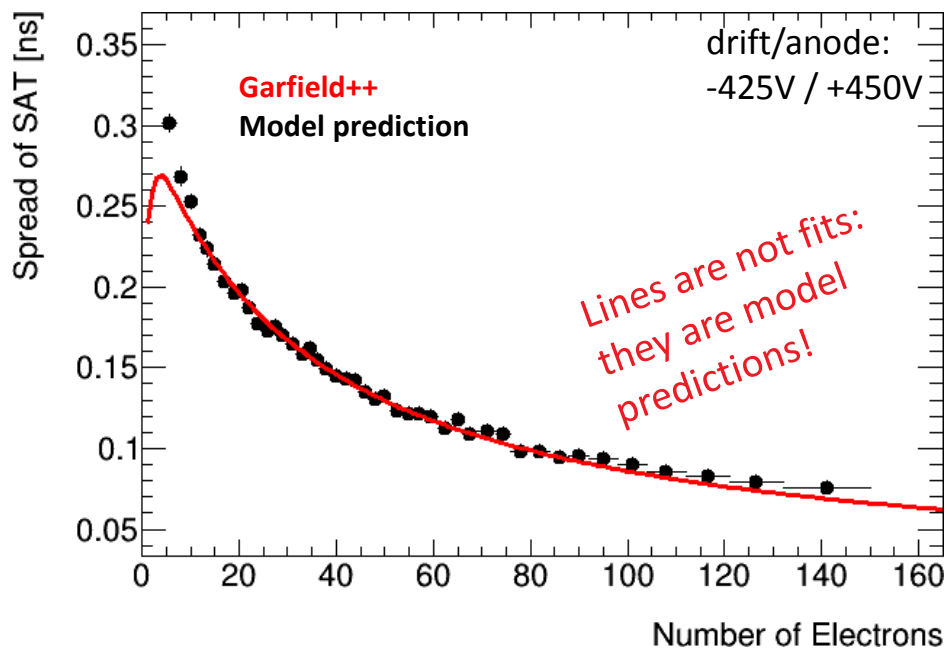


We can describe and explain the SAT dependence on the number of avalanche's electrons (i.e. on the e-peak size)

- The other parameters of the model are: the drift velocity of the photoelectron and the first Townsend coefficient.
- The model treats the number of electrons in an avalanche as continue variable.

Understood in terms of phenomenological model(2)

We can describe and explain the Resolution dependence on the length of the avalanche and on the number of avalanche's electrons (i.e. on the e-peak size)



The model describes SAT and Resolution

a) vs. avalanche length &

b) vs. number of electrons in avalanche

(i.e. vs. e-peak charge)

→ Before and after the mesh

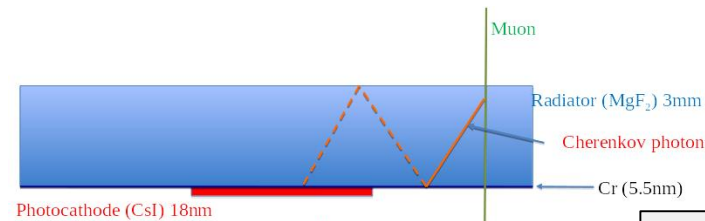
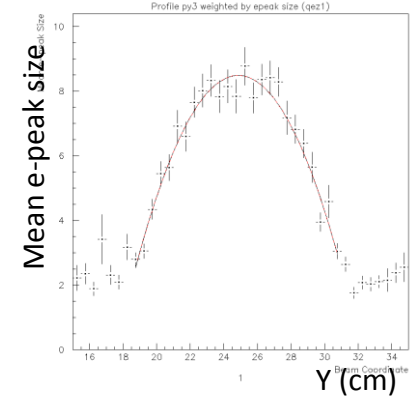
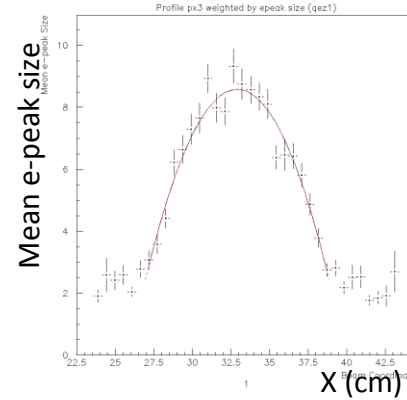
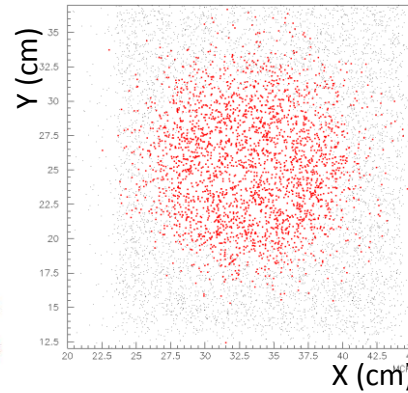
Not only averages and RMS, but full distributions,
vs. values of operational parameters (e.g., drift
voltage)

arXiv:1901.10779v1 [physics.ins-det]

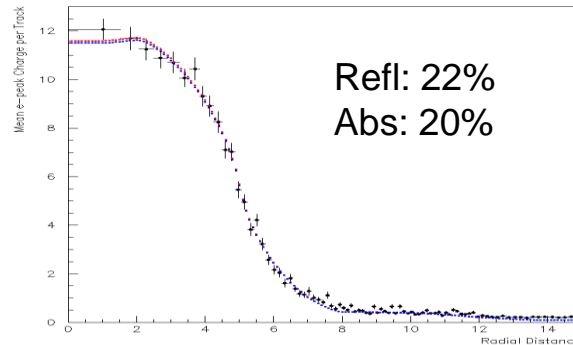
3. Estimation of the No of pes per MIP

A consistent and unbiased procedure to estimate the number of photoelectrons per MIP(1)

Precise alignment based on the charge-weighted beam profile



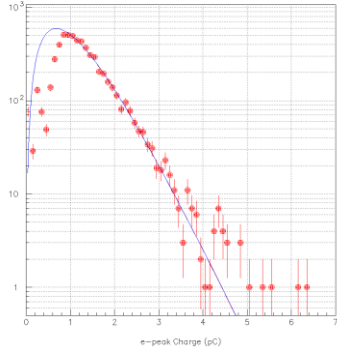
Determination of the anode geometrical acceptance taking into account reflections



Mean charge per track (pC) vs the track radial distance (mm)

A consistent and unbiased procedure to estimate the number of photoelectrons per MIP(2)

Determination of the charge distribution parameters when the PICOSEC MM responds to a single-pe using UV calibration data



A Polya fit to the single-pe charge distribution

$$P_{spe}(Q; a = b = \theta + 1, \bar{Q}_e) dQ = \frac{1}{Q_e} \frac{(\theta + 1)^{(\theta + 1)} (Q / \bar{Q}_e)^\theta}{\Gamma(\theta + 1)} e^{-(\theta + 1)Q / \bar{Q}_e} dQ$$

$$E[Q_{spe}] = \bar{Q}_e = \langle Q_e \rangle$$

$$V[Q_{spe}] = \frac{1}{\theta + 1} \langle Q_e \rangle^2 = RMS^2$$

RMS	Mean
0.6433	1.0668
0.6498	1.1102
0.6452	1.117
0.6388	1.0786
0.6398	1.028
0.64305	1.0118

Take into account systematic errors due to threshold effects

Fit the charge distribution of the PICOSEC response to muons

If N is the mean number of pes produced per muon track, then a muon passing through the radiator at distance R from the anode center will result to a PICOSEC signal with charge Q.

Q follows a p.d.f. $F(Q, R; N)$ which can be expressed using the geometrical acceptance $A(R)$, as a convolution of a Poissonian distribution with mean $N \cdot A(R)$

$$\Pi(N_{pe}; N, A(R)) = \frac{[N \cdot A(R)]^{N_{pe}}}{N_{pe}!} \cdot \exp[-N \cdot A(R)]$$

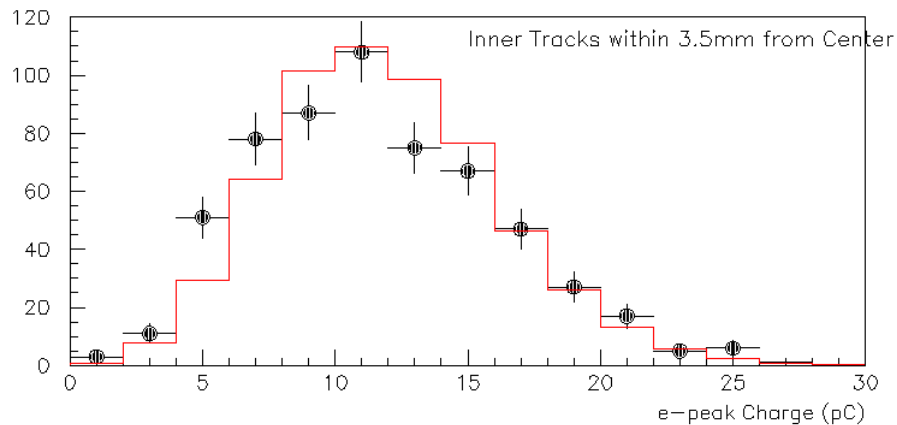
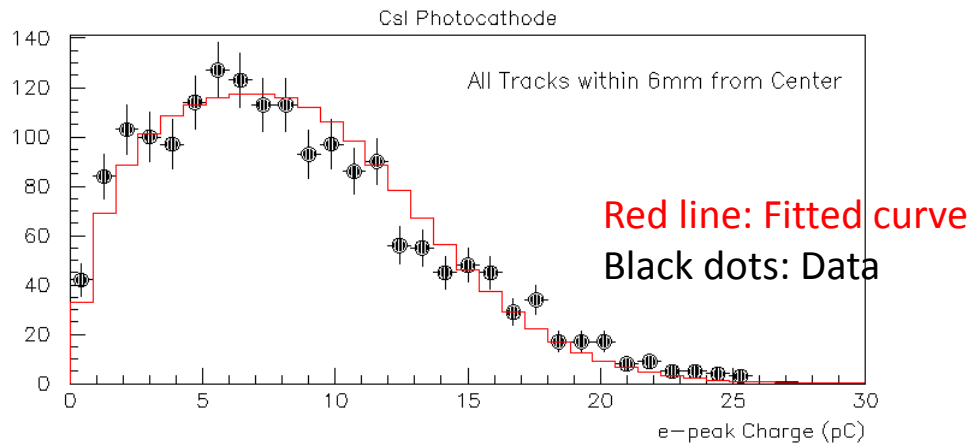
and the multi-Polya distribution

$$P(Q; N_{pe}, \theta, \bar{Q}_e) = \frac{P_{spe} \otimes P_{spe} \dots \otimes P_{spe}}{N_{pe} \text{ times}} = \frac{1}{Q_e} \frac{(\theta + 1)^{N_{pe}(\theta + 1)} (Q / \bar{Q}_e)^{N_{pe}(\theta + 1) - 1}}{\Gamma(N_{pe}(\theta + 1))} \cdot \exp[-(\theta + 1) \cdot Q / \bar{Q}_e]$$

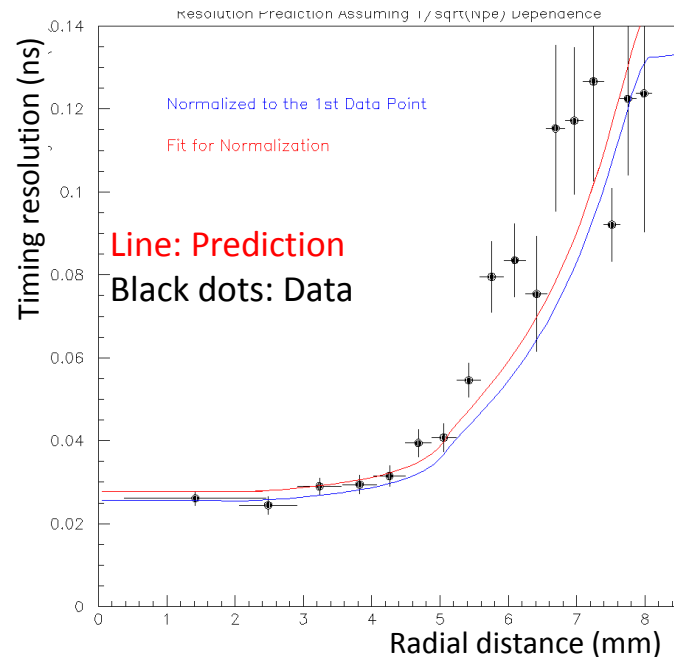
as

$$F(Q, R; N) = \sum_{N_{pe}=0}^{\infty} \Pi(N_{pe}; N, A(R)) \cdot P(Q; N_{pe}, \theta, \bar{Q}_e)$$

A consistent and unbiased procedure to estimate the number of photoelectrons per MIP(3)



**$11.5 \pm 0.4(\text{stat}) \pm 0.5(\text{syst})$
photoelectrons per muon track**



Resolution prediction vs distance from the anode center, assuming $1/\sqrt{Npe}$ dependence

4. Towards a robust, large-scale detector

Detector stability

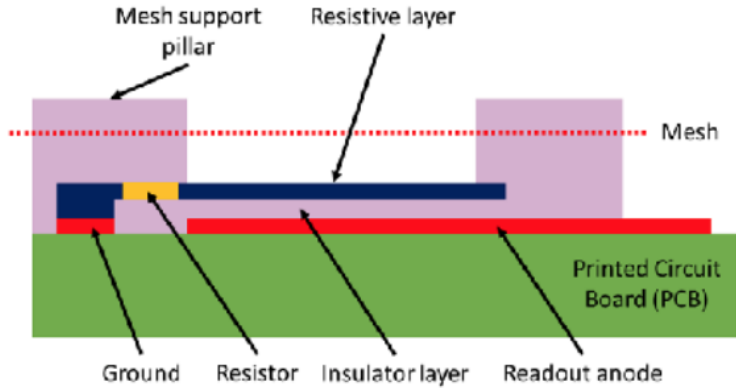
Photocathode robustness

Large area coverage

Detector stability – Resistive Micromegas

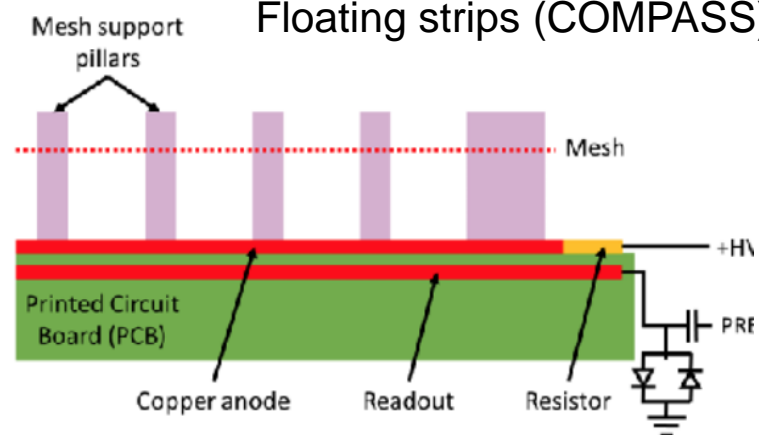
Best resolution was at voltages which give high currents on anode: **robust anode**

Resistive strips (MAMMA)



Readout beneath resistive layer: picks up signal from above

Floating strips (COMPASS)



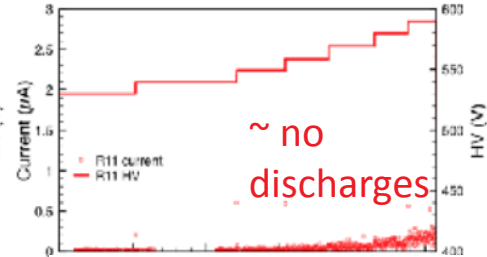
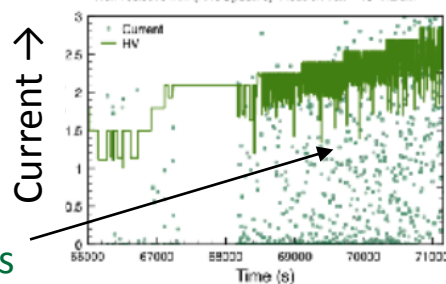
Copper Layer to HV via resistor; Readout “floating”

Resistive readouts operate stably at high gain in neutron fluxes of 10^6 Hz/cm².

T. Alexopoulos *et al.*,
NIMA 640 (2011) 110-118.

discharges

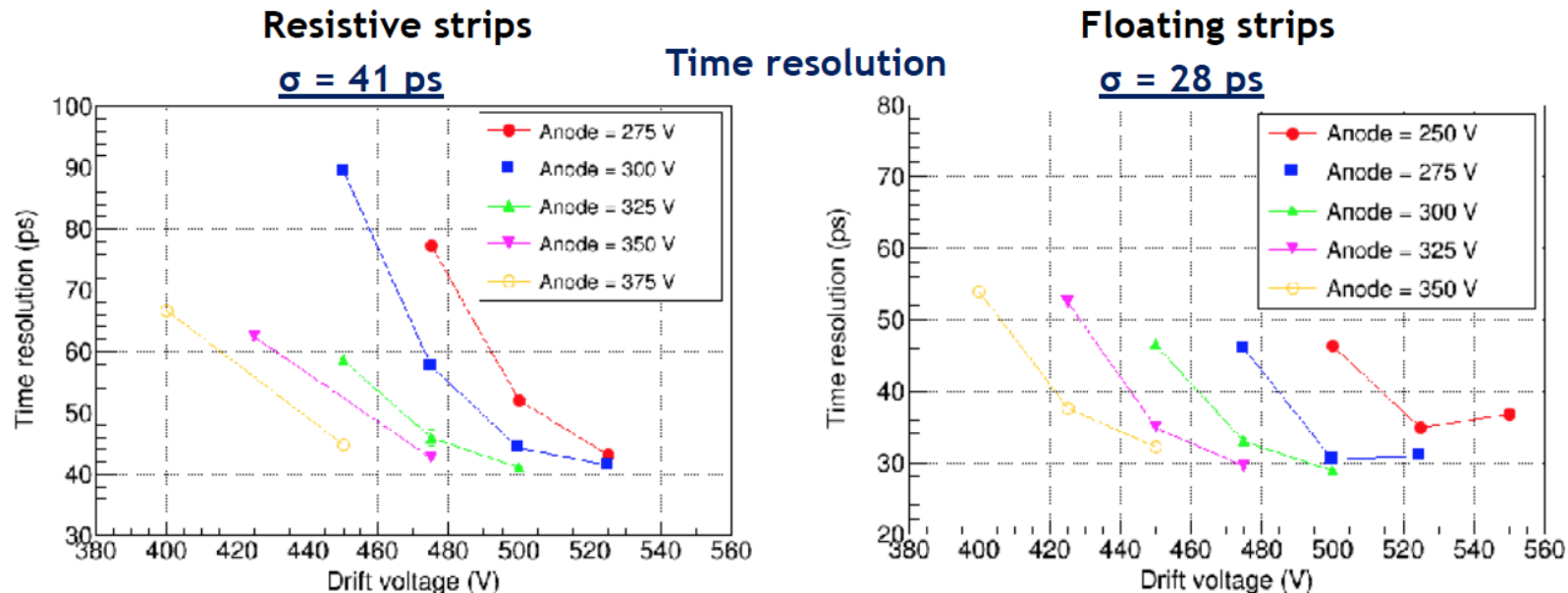
Non resistive ← MAMMA results → With resistive strip



Irradiation time →

Detector stability – Resistive Micromegas

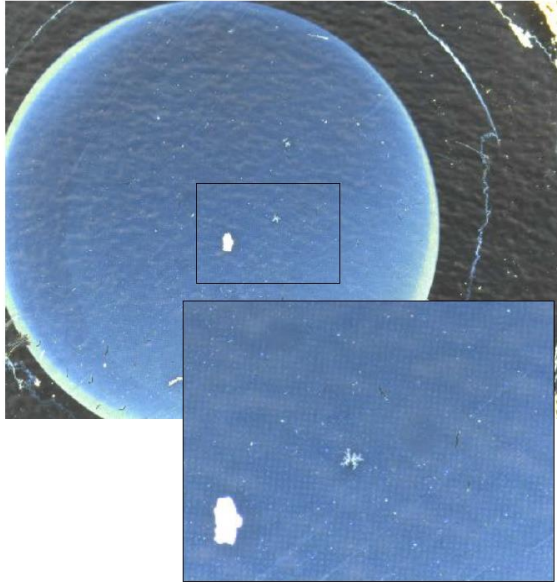
Beam results with protected anodes



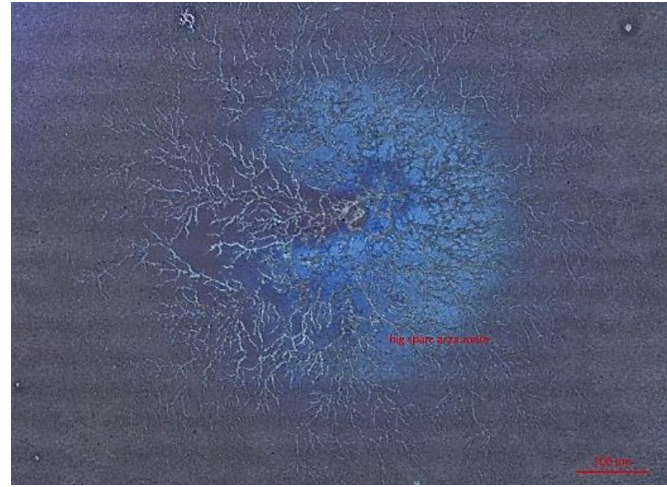
- Values not far from the Picosec bulk readout.
 - Resistive strips: **41 ps** (10 M Ω/\square), **35 ps** (300 k Ω/\square).
 - Floating strips: **28 ps** (25 M Ω).
- Resistive readouts worked during hours in intense pion beam.

Photocathode robustness – Problems with CsI

CsI sensitive to humidity, ion backflow and sparks



Ion backflow on CsI



CsI photocathode after spark

Photocathode robustness – Protection and alternatives

Photocathode robustness preserves QE and thus detector efficiency and timing resolution during long-period operation

- **Protection layers on CsI and alternative photocathode materials** (Metallic, DLC, B_4C , nano diamond powder, CVD diamond) were tested
- For each material, the working point with the best time resolution has to be determined
- Inherently robust materials, but with lower QE

Most promising performance results for non-CsI are from **Diamond-Like Carbon (DLC)**, which also seems robust:

- atmospheric conditions for a few months
- irradiated with pions, in a resistive MM prototype → minimal reduction of Npe/MIP

3mm MgF_2 + DLC of different thicknesses:



Photocathode robustness – Diamond-like Carbon

- 2.5 nm DLC time resolution up to 34 ps observed
- Results repeatable in independent samples and measurements
- Additional tests with heating treatment under N₂ and H₂
- Additional ageing tests under pions
- Samples survived rough transport from China

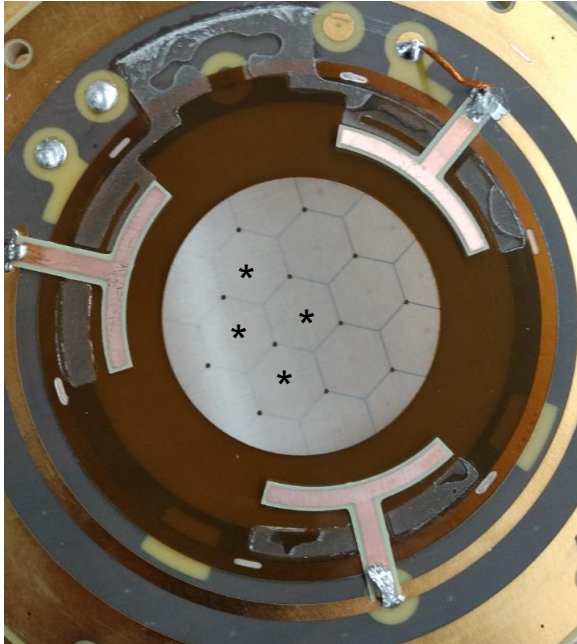
Thickness of DLC film (nm)	Npe/per muon	Detection efficiency for muons
1	Bad	Bad
2.5	3.7	97%
5	3.4	94%
7.5	2.2	70%
10	1.7	68%
5 nm Cr + 18 nm Csl	7.4	100%

PRELIMINARY

2.5 nm DLC in Bulk MM

A/D Voltage	Time Res. (ps)
250/550	37
250/575	34
275/525	38
275/550	34
300/500	39
300/525	34

Large-area coverage - Multi-pad MicroMegas



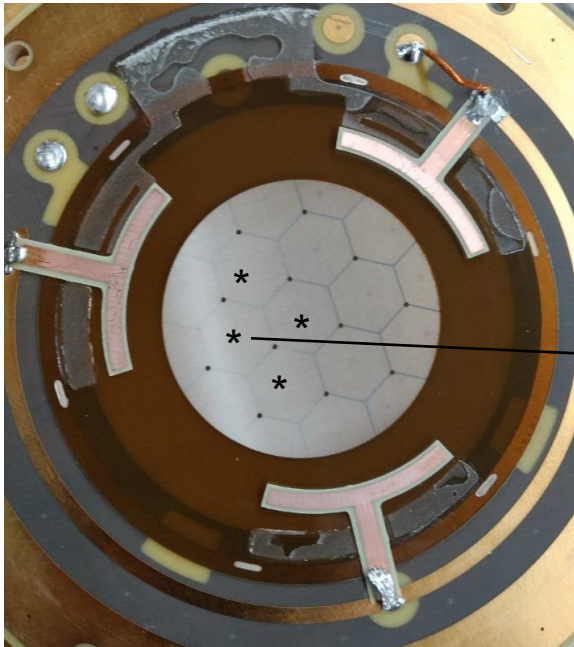
- Like the single-pad ($\text{MgF}_2/\text{CsI}/\text{bulkMM}/\text{COMPASS gas}$) PICOSEC which achieved 24ps per MIP

- Hexagonal pads 5mm side
- Readout 4 pads \rightarrow 2 oscilloscopes

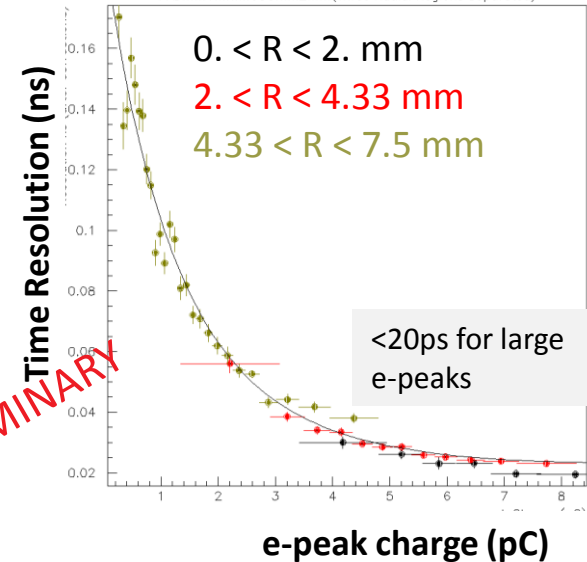
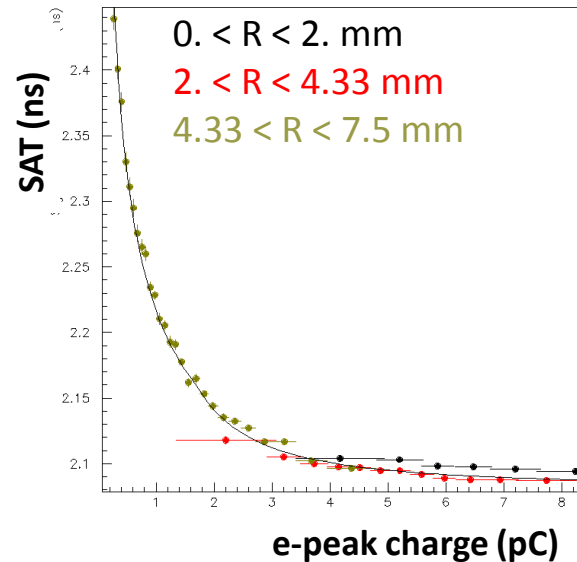
Large-area coverage - Multi-pad MicroMegas

Multi-pad: individual pad response vs. R

- Study response vs. R : distance of track impact from pad center
 - $0 < R < 2\text{mm}$: full Cherenkov cone (3mm) inside pad
 - $2 < R < 4.33\text{mm}$: Cherenkov cone (3mm) mostly inside pad
 - $4.33 < R < 7.5\text{mm}$: Cherenkov cone (3mm) mostly outside pad



Hexagonal pads 5mm side



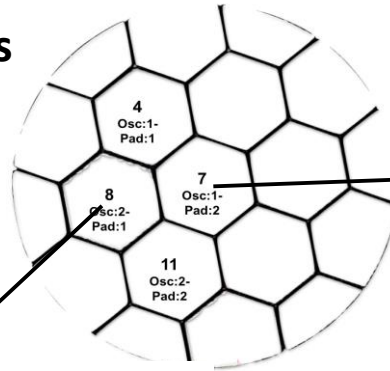
e-peak charge should have all info about where is Cherenkov cone compared to pad. Indeed, universal curves vs. e-peak charge:

Large-area coverage - Multi-pad MicroMegas

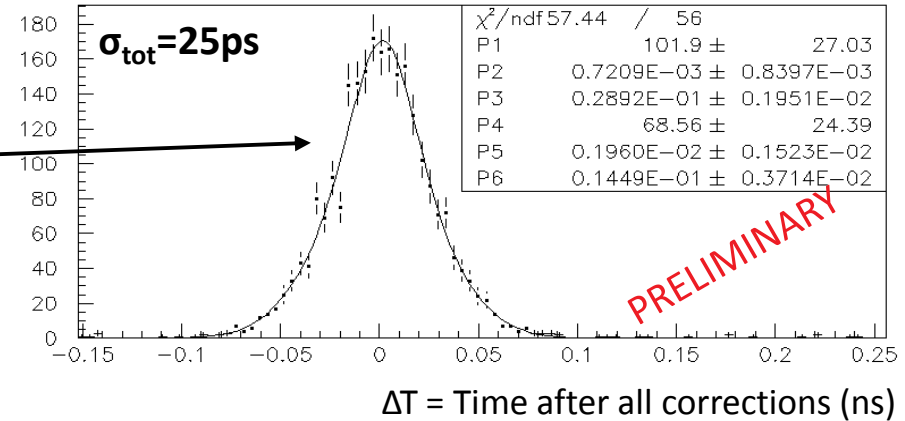
Multi-pad: Same resolution as single-pad

At center of each pad ($0 < R < 2\text{mm}$):

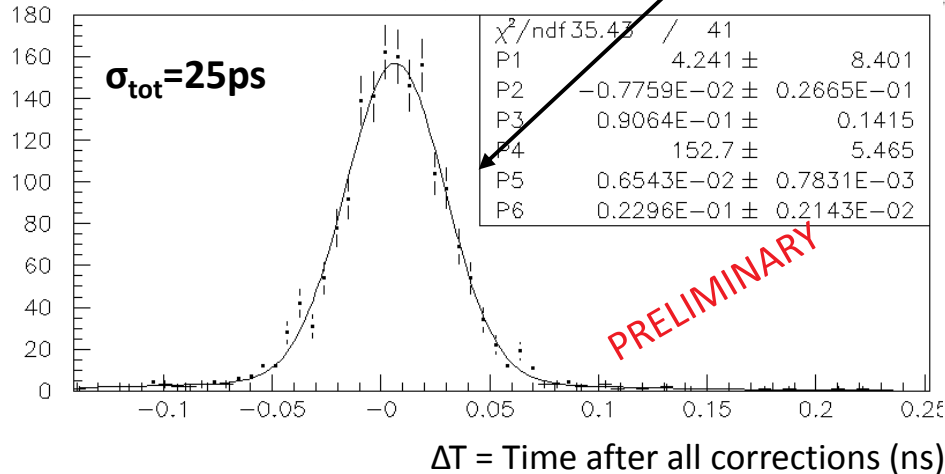
Timing resolution of **25ps** for all pads



Individual pad response



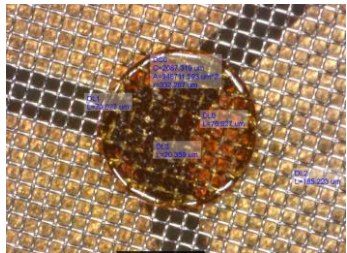
Individual pad response



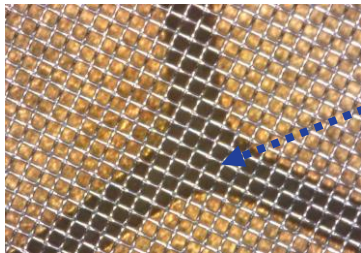
Large-area coverage - Multi-pad MicroMegas

Individual pad responses for tracks falling around the “three-pads” region

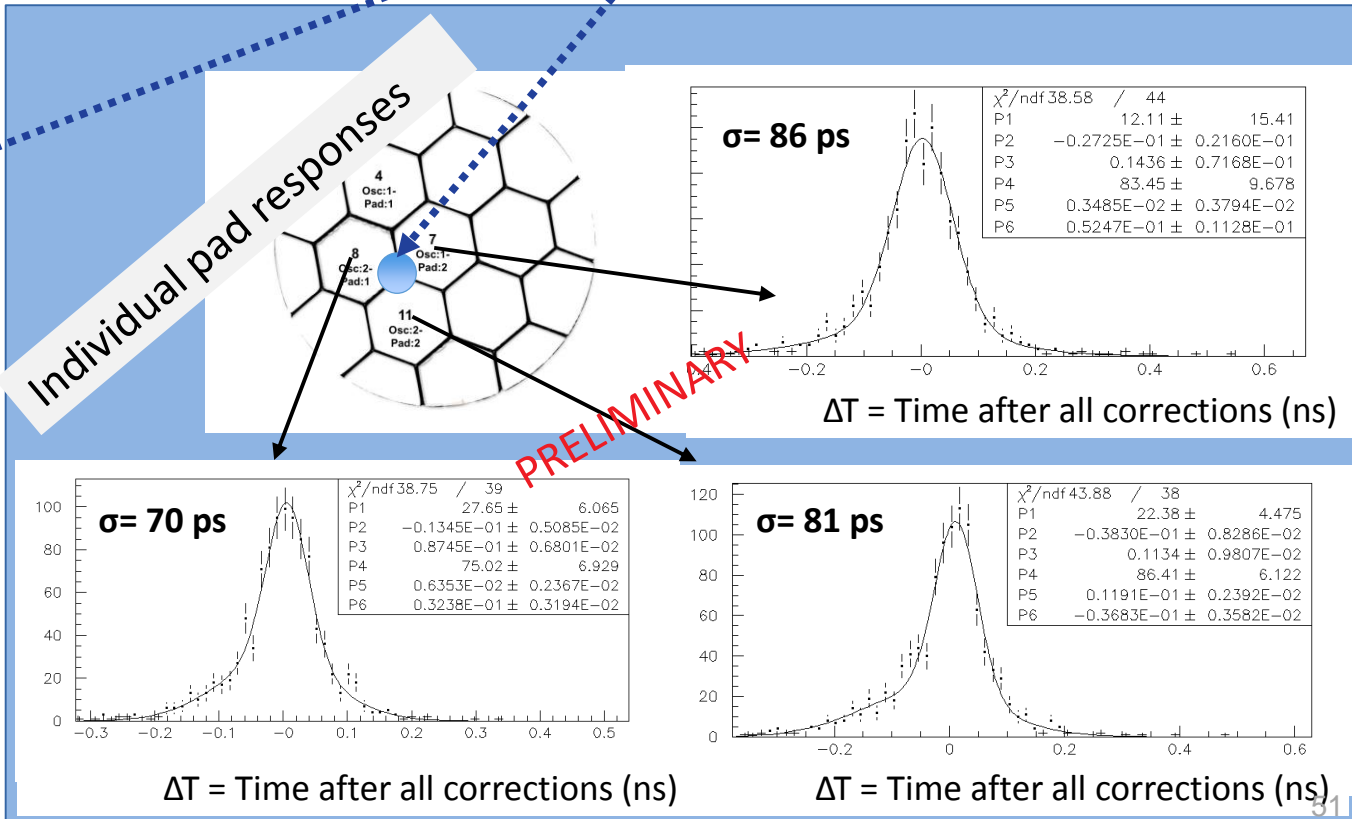
These are not the easiest regions



Pillars of $\sim 650\mu\text{m}$ diameter



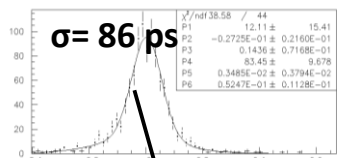
200 μm inter-pad space



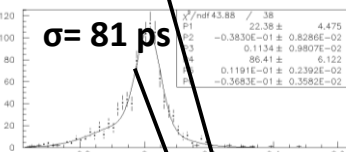
Large-area coverage - Multi-pad MicroMegas

Combining pads for tracks falling around the “three-pads” region

Individual pad responses



ΔT = Time after all corrections (ns)

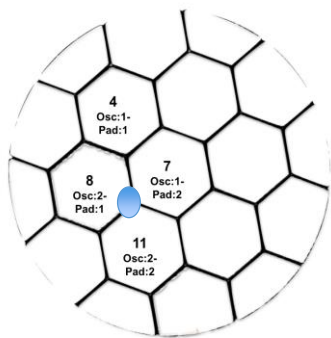


ΔT = Time after all corrections (ns)

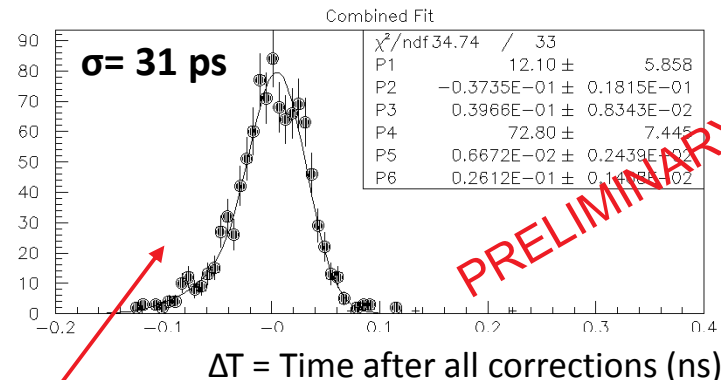


ΔT = Time after all corrections (ns)

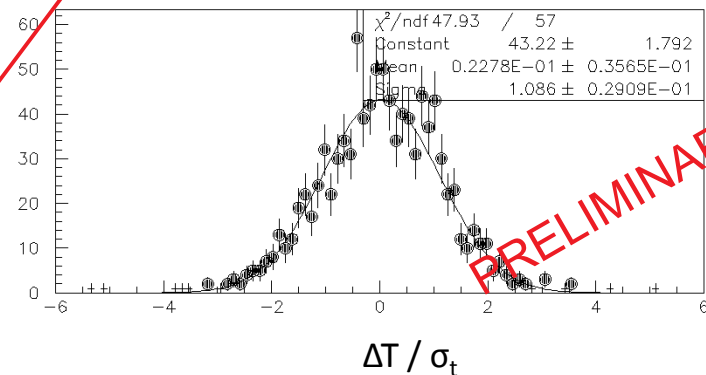
Combining pads event-by-event



$$\chi^2 = \sum_{i=1,3} \frac{\left([t_i - \{SAT\}(R_i, \theta_i) - \{SAT\}(R_i, 90^\circ)] - \{SL(Q)\} - \hat{t} \right)^2}{(Res(Q_i))^2}$$



ΔT = Time after all corrections (ns)



Similar results all across the area covered by the 4 pads

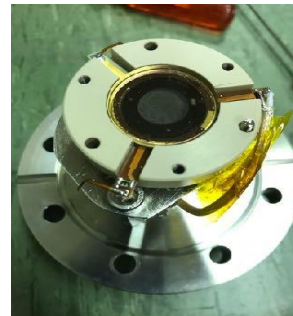
Naive estimation:
 $\langle \sigma \rangle / \sqrt{3} \approx 45 \text{ ps}$

Large-area coverage

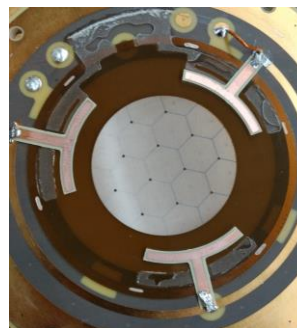
Scaling up multi-channel PICOSEC

Several variants of multi-channel PICOSEC prototypes in development / under test, associated with scaling to larger areas:

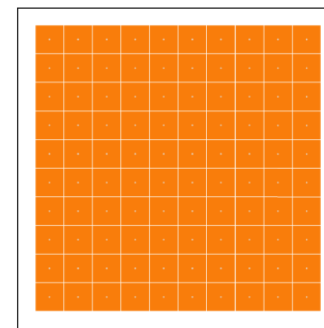
- Signal routing and sharing across pads
- Multi-channel amplifiers and digitizers
- Resistive multi-pad anode
- Detector uniformity
- Large Cherenkov radiators
- Mechanics to preserve precise gaps
- Compact detector vessel
- ...



Single pad \varnothing 1cm



Multi-pad \varnothing 1cm



10 x 10 module

Conclusions

- **PICOSEC MicroMegs: a detector with precise timing:**
 - Single-channel prototype in Laser and Particle beams
 - 76ps for single photoelectrons, 24ps resolution for timing MIPs
- **A well-understood detector:**
 - reproduce observed behavior with detailed simulations and a phenomenological model: valuable tool for parameter-space exploration
- **Efficient photocathode**
 - consistent and unbiased procedure to estimate the number of photoelectrons per MIP
- **Towards a large-scale detector: multi-channel, robustness, photocathodes**
 - response of multi-channel PICOSEC prototype: similar precision as the single-channel prototype, for any impact point of a MIP, progress towards a robust detector

Thank you

Stage 3 – Electronics (2) – technique is consistent and unbiased

See RD51 Notes 2017-011
And 2018-004 (Kostas Paraschou's thesis)

$\bar{S}(t)$

$$P_{Q_{tot}=Q}(\tau_1, \dots, \tau_k, q_1, \dots, q_k; k) = \frac{\delta\left(Q - \sum_{i=1}^k q_i\right) \cdot R(k) \cdot \prod_{i=1}^k \Phi(\tau_i; k) \cdot \prod_{i=1}^k G(q_i)}{N(k)}$$

where

$$N(k) = \int_0^\infty \dots \int_0^\infty \delta\left(Q - \sum_{i=1}^k q_i\right) \cdot R(k) \cdot \prod_{i=1}^k G(q_i) dq_1 \dots dq_k$$

$$\begin{aligned} \langle S(t) \rangle_{Q_{tot}=Q} &= \sum_{k=1}^{\infty} R(k) \int_0^\infty \dots \int_0^\infty \sum_{i=1}^k q_i f(t - \tau_i) \cdot \delta\left(Q - \sum_{i=1}^k q_i\right) \cdot \\ &\quad \cdot \prod_{j=1}^k \Phi(\tau_j; k) \cdot \prod_{j=1}^k G(q_j) dq_1 \dots dq_k d\tau_1 \dots d\tau_k \end{aligned}$$

$$\begin{aligned} \langle S(t) \rangle_{Q_{tot}=Q} &= \sum_{k=1}^{\infty} R(k) \sum_{i=1}^k \int_0^\infty f(t - \tau_i) \Phi(\tau_i; k) d\tau_i \cdot \\ &\quad \cdot \int_0^\infty \dots \int_0^\infty q_i \cdot \delta\left(Q - \sum_{i=1}^k q_i\right) \cdot \prod_{j=1}^k G(q_j) dq_1 \dots dq_k \end{aligned}$$

$$\langle q_i \rangle_{Q=\sum_{j=1}^k q_j} = \frac{\int_0^\infty \dots \int_0^\infty q_i \cdot \delta\left(Q - \sum_{i=1}^k q_i\right) \cdot \prod_{j=1}^k G(q_j) dq_1 \dots dq_k}{N(k)}$$

$$\begin{aligned} \langle S(t) \rangle_{Q_{tot}=Q} &= \sum_{k=1}^{\infty} R(k) N(k) \sum_{i=1}^k \int_0^\infty f(t - \tau_i) \Phi(\tau_i; k) d\tau_i \cdot \\ &\quad \cdot \int_0^\infty \dots \int_0^\infty \frac{q_i \cdot \delta\left(Q - \sum_{i=1}^k q_i\right) \cdot \prod_{j=1}^k G(q_j)}{N(k)} dq_1 \dots dq_k \end{aligned}$$

$$\langle S(t) \rangle_{Q_{tot}=Q} = \sum_{k=1}^{\infty} R(k) N(k) \cdot \sum_{i=1}^k \langle q_i \rangle_{Q=\sum_{j=1}^k q_j} \int_0^\infty f(t - \tau_i) \Phi(\tau_i; k) d\tau_i$$

$$\int_0^\infty f(t - \tau_i) \Phi(\tau_i; k) d\tau_i = \int_0^\infty f(t - \tau) \Phi(\tau; k) d\tau$$

$$\langle S(t) \rangle_{Q_{tot}=Q} = \sum_{k=1}^{\infty} R(k) N(k) \int_0^\infty f(t - \tau) \Phi(\tau; k) d\tau \sum_{i=1}^k \langle q_i \rangle_{Q=\sum_{j=1}^k q_j}$$

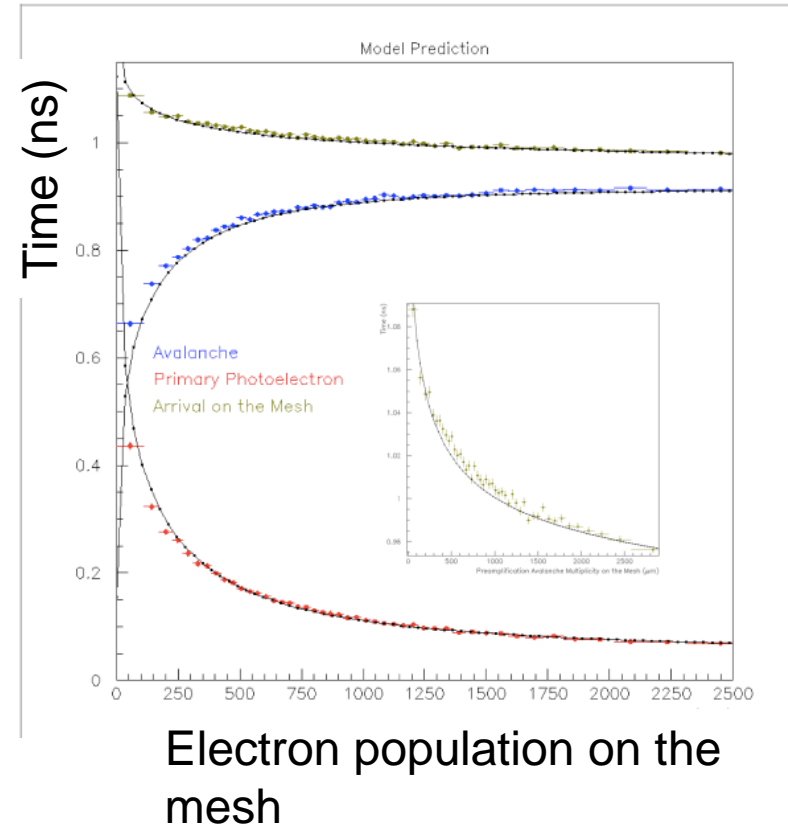
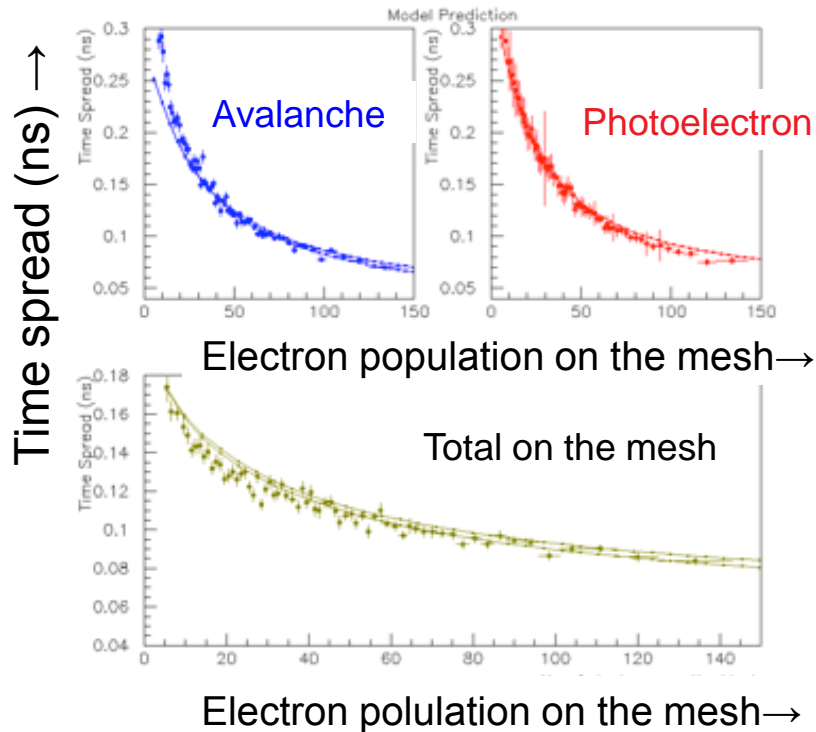
$$= Q \sum_{k=1}^{\infty} R(k) N(k) \int_0^\infty f(t - \tau) \Phi(\tau; k) d\tau$$

$$= Q \int_0^\infty f(t - \tau) \left\{ \sum_{k=1}^{\infty} R(k) N(k) \Phi(\tau; k) \right\} d\tau$$

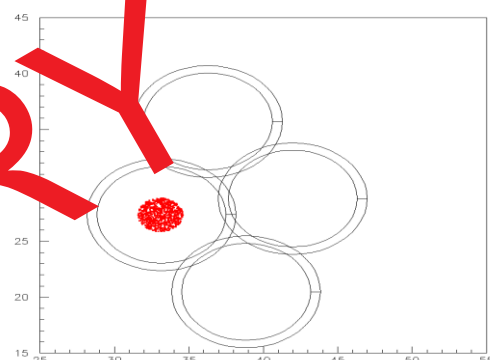
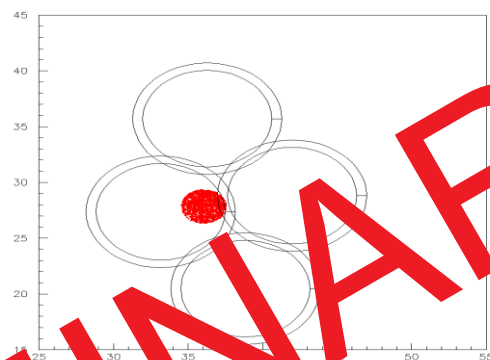
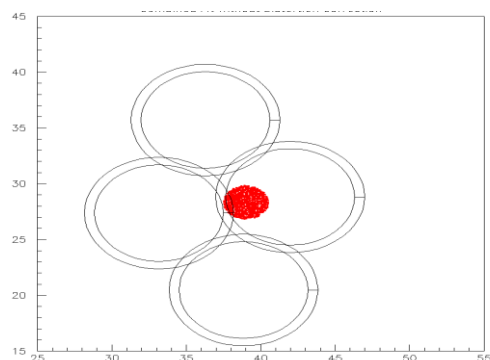
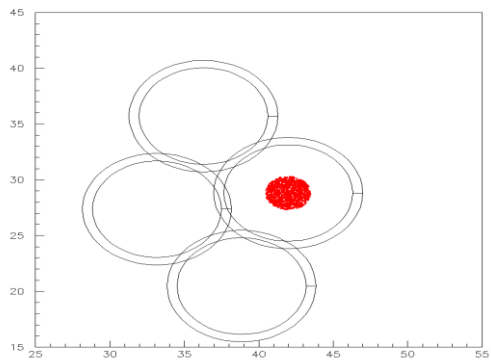
$$\langle \Phi(\tau) \rangle_{Q_{tot}=Q} = \sum_{k=1}^{\infty} R(k) N(k) \Phi(\tau; k)$$

Understood in terms of phenomenological model

- Known in literature that quenchers in the gas-mix increase drift velocity →
- Model:** assume a time-gain per inelastic interaction compared to elastic interactions



Multi- pad: Tracks are selected within a circle of 1.5 mm radius

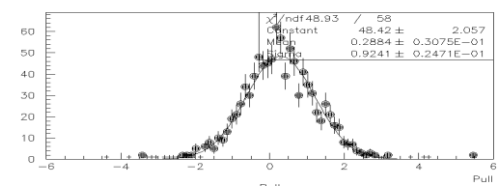
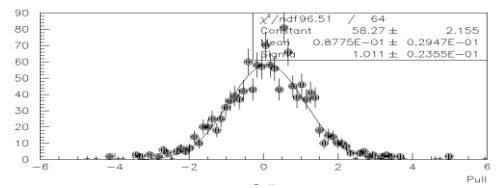
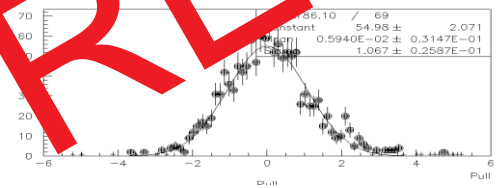
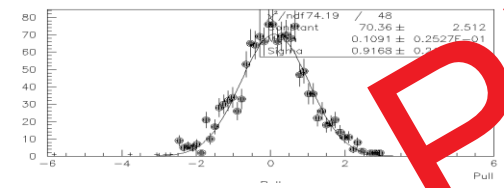
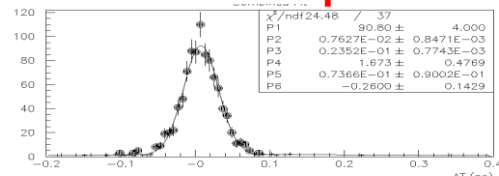
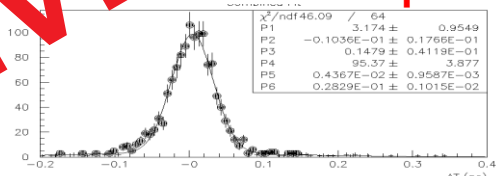
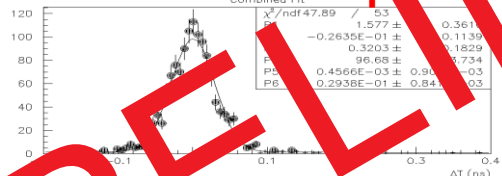
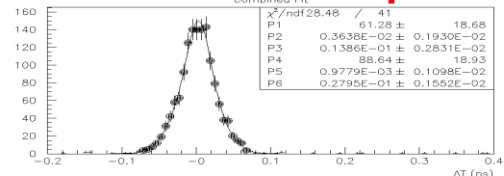


$\mu = 1.6 \pm 2 \text{ ps}$
 $\sigma = 25 \pm 1.5 \text{ ps}$

$\mu = 0 \pm 2 \text{ ps}$
 $\sigma = 31 \pm 1.5 \text{ ps}$

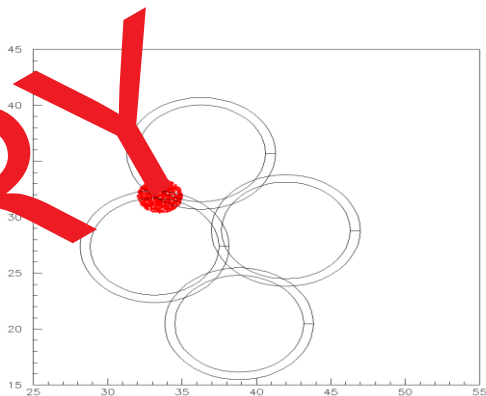
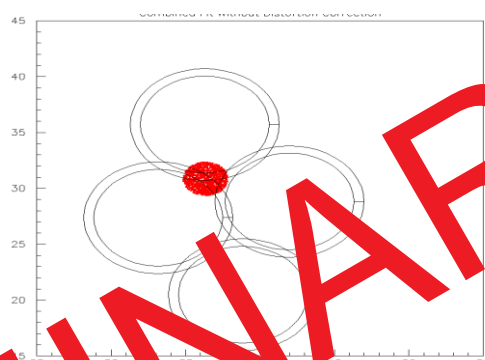
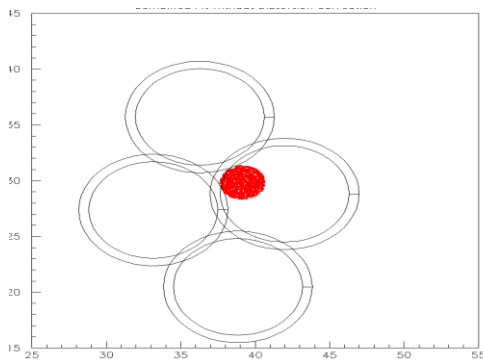
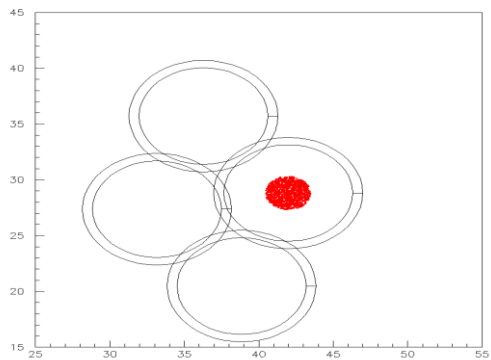
$\mu = 2 \pm 2 \text{ ps}$
 $\sigma = 31 \pm 1.5 \text{ ps}$

$\mu = 5 \pm 2 \text{ ps}$
 $\sigma = 25 \pm 1.5 \text{ ps}$



PRELIMINARY

Multi- pad: Tracks are selected within a circle of 1.5 mm radius

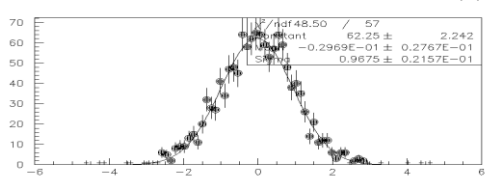
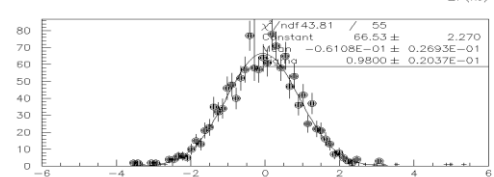
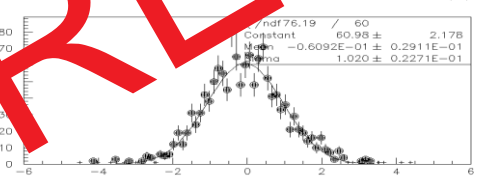
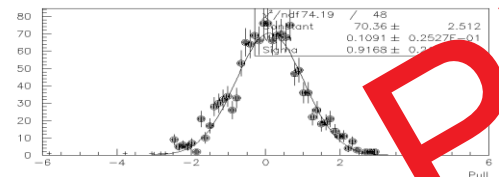
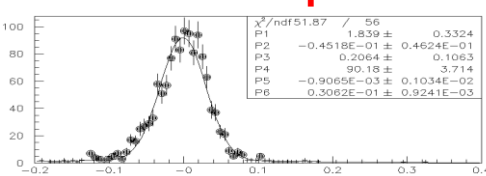
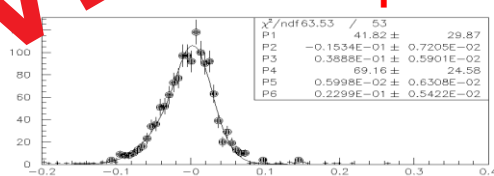
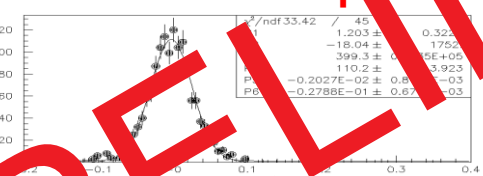
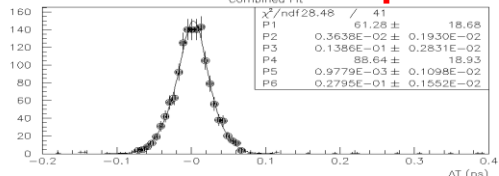


$\mu = 1.6 \pm 2 \text{ ps}$
 $\sigma = 25 \pm 1.5 \text{ ps}$

$\mu = -2 \pm 2 \text{ ps}$
 $\sigma = 29 \pm 1.5 \text{ ps}$

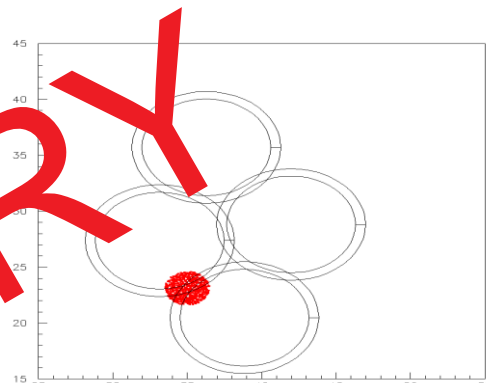
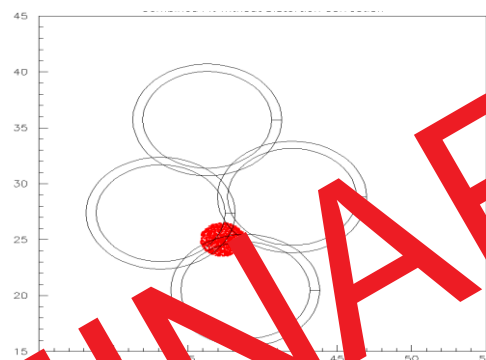
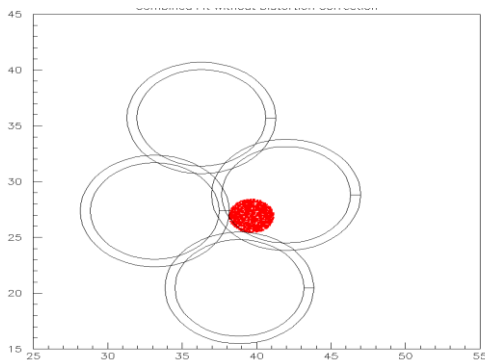
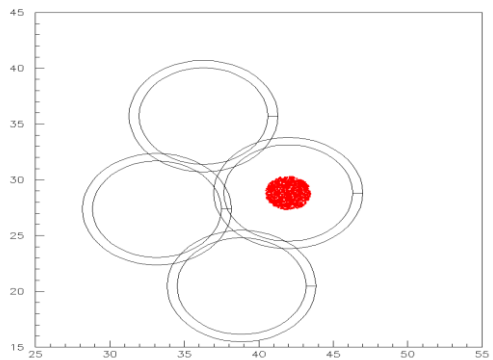
$\mu = 4 \pm 2 \text{ ps}$
 $\sigma = 32 \pm 1.5 \text{ ps}$

$\mu = -1.5 \pm 2 \text{ ps}$
 $\sigma = 33 \pm 1.5 \text{ ps}$



PRELIMINARY

Multi- pad: Tracks are selected within a circle of 1.5 mm radius

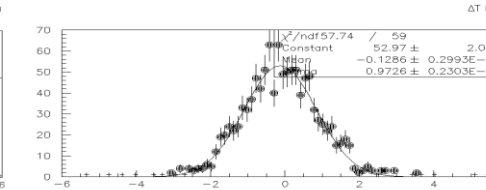
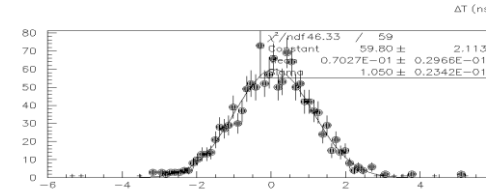
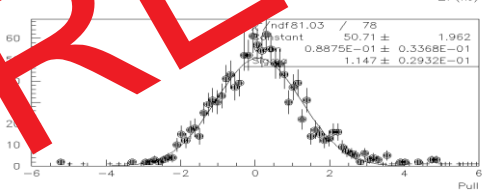
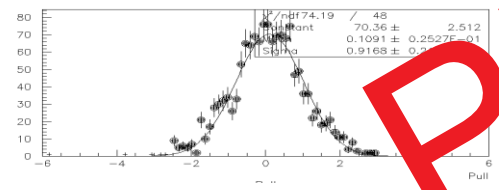
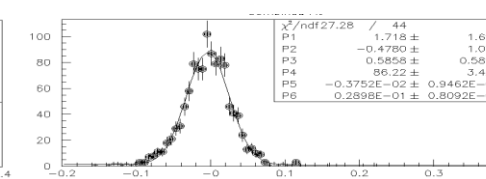
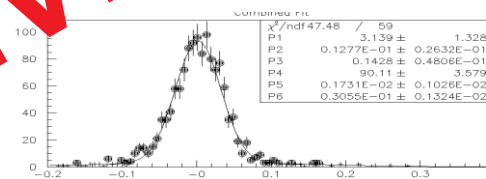
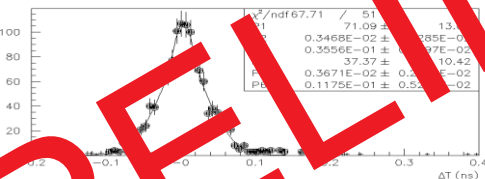
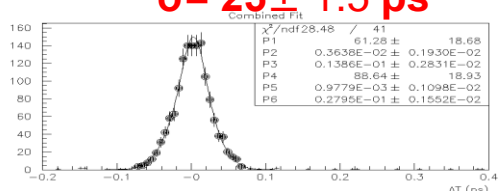


$\mu = 1.6 \pm 2 \text{ ps}$
 $\sigma = 25 \pm 1.5 \text{ ps}$

$\mu = 3 \pm 2 \text{ ps}$
 $\sigma = 32 \pm 1.5 \text{ ps}$

$\mu = 1 \pm 2 \text{ ps}$
 $\sigma = 33 \pm 1.5 \text{ ps}$

$\mu = 4 \pm 2 \text{ ps}$
 $\sigma = 31 \pm 1.5 \text{ ps}$



PRELIMINARY